Extensive surface pedogenic alteration of the Martian Noachian crust suggested by plateau phyllosilicates around Valles Marineris

Laetitia Le Deit,[1] Jessica Flahaut,[2] Cathy Quantin,[2] Ernst Hauber,[1] Daniel Mège,[3,4]
Olivier Bourgeois,[4] Joanna Gurgurewicz,[3,5] Marion Massé,[3,6] and R. Jaumann[1]

[1] Thousands of phyllosilicate-rich outcrops, mainly iron or magnesium-rich are exposed on Noachian terrains in the Martian southern highlands. We analyzed 90 CRISM observations and more than a hundred HiRISE images located on the plateaus surrounding Valles Marineris. We mapped an extensive Al- and Fe/Mg-phyllosilicate-rich formation covering at least $\sim$197,000 km^2, for which we introduce the name "Plateau Phyllosilicates." Tens of meters in thickness, this light-toned formation crops out at various elevations on top of the Noachian units Npl$_1$ and Npl$_2$, as flat exposures on plateaus and along scarps such as valley walls, chasma walls, pit walls and impact crater rims. The Fe/Mg-phyllosilicate-rich lower member of the formation is composed of Fe/Mg-smectites (nontronite, saponite) and vermiculite. The Al-phyllosilicate-rich upper member of the formation contains Al-smectites (montmorillonite, beidellite) and locally kaolinite and/or halloysite. We suggest that the Plateau Phyllosilicates were mainly formed by pedogenesis related to the weathering of the Noachian bedrock by percolation of meteoric water or melted snow under a temperate and subarid climate during the Noachian Epoch in an alkaline to neutral environment. Kaolinite and/or halloysite may have formed in areas of more intense drainage at the surface under slightly acidic environments during the Noachian and Hesperian Epochs. Fluvial activity and deuteric alteration may have locally contributed to the genesis of phyllosilicates. This study suggests that the alteration of the Noachian basement of the plateaus surrounding Valles Marineris was widespread during the Noachian Epoch, and was still active during the Hesperian Epoch even though the water availability was limited.

1. Introduction

[2] Several thousands of phyllosilicate-rich outcrops are exposed in the Noachian terrains of the Martian southern highlands [e.g., *Poulet et al.*, 2005; *Bibring et al.*, 2006; *Poulet et al.*, 2007; *Mustard et al.*, 2008; *Murchie et al.*, 2009a; *Carter et al.*, 2009; *Ehlmann et al.*, 2009; *Wray et al.*, 2009]. Phyllosilicates are alteration minerals that signify past aqueous activity of the planet Mars. The study of their nature, distribution, and geological context may provide fundamental constraints on the environmental and climatic conditions in which they formed. Most of the phyllosilicates detected so far contain iron and/or magnesium and correspond to smectite clays such as nontronite or saponite [e.g., *Bibring et al.*, 2006]. Other phyllosilicates such as Al-smectites (e.g., Al-montmorillonite), kaolinites, chlorite, prehnite, serpentine, and potassium micas such as illite or muscovite have also been detected at the Martian surface [e.g., *Poulet et al.*, 2005; *Bibring et al.*, 2006; *Loizeau et al.*, 2007; *Bishop et al.*, 2008a; *Wray et al.*, 2008; *Ehlmann et al.*, 2009; *Murchie et al.*, 2009a].

[3] Iron and/or magnesium smectite clays mainly occur in four different types of geological formations [e.g., *Murchie et al.*, 2009a]. Formation #1, for which we suggest the collective name "Impact Phyllosilicates," is spatially associated with impact craters. It corresponds to impact megabreccia and light-toned units exposed in central pits, uplifts and ejecta of impact craters. It has been detected in many outcrops of the southern highlands including Ritchey Crater and many unnamed craters on Noachian and Hesperian-aged terrains [*Milliken*, 2007; *Loizeau et al.*, 2012; C. Quantin et al., Composition and structure of the subsurface in the vicinity of Valles Marineris as revealed by central uplift of

[1]Institute of Planetary Research, German Aerospace Center, Berlin, Germany.
[2]Laboratoire de Géologie de Lyon, UMR 5276, CNRS, Université Claude Bernard Lyon 1, Ecole Normale Supérieure de Lyon, Villeurbanne, France.
[3]WROONA Group, Institute of Geological Sciences, Polish Academy of Sciences, Research Centre, Wrocław, Poland.
[4]Laboratoire de Planétologie et Géodynamique, UMR 6112, CNRS, Université de Nantes, Nantes, France.
[5]Space Research Centre, Polish Academy of Sciences, Warsaw, Poland.
[6]Lunar and Planetary Laboratory, University of Arizona, Tucson, Arizona, USA.
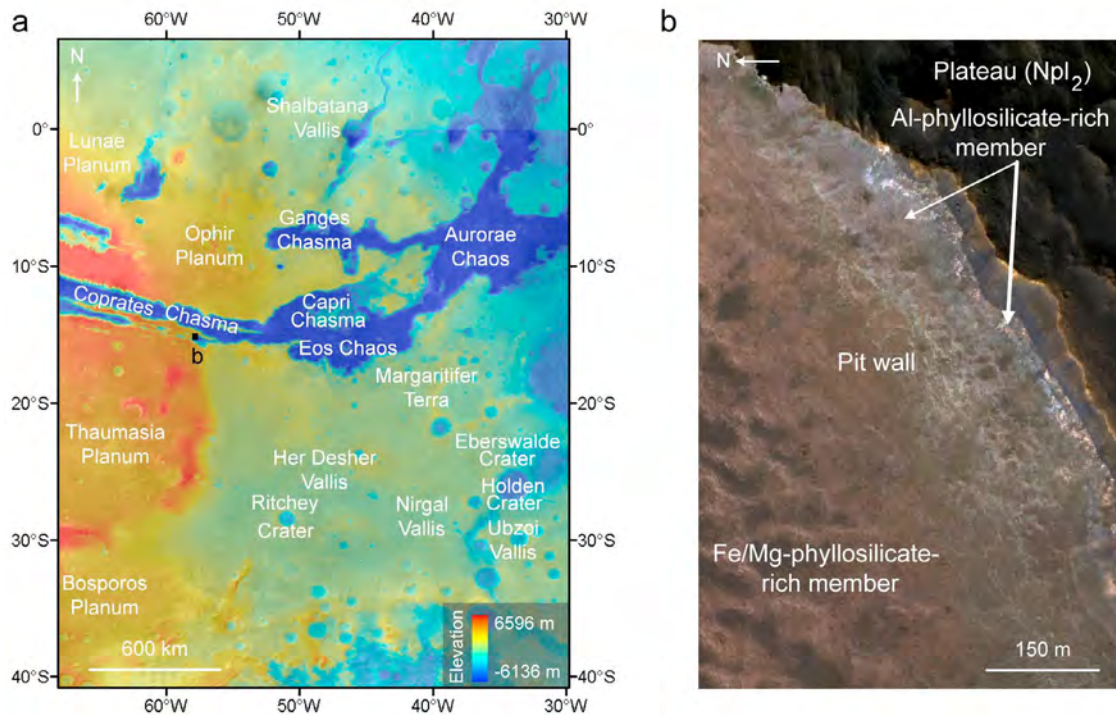
Figure 1. (a) Topographic map of the study area (MOLA digital elevation model at 128 pixels/deg overlapping a mosaic of MOC images at 256 pixels/deg). Location of Figure 1b is indicated. (b) Al-phyllosilicate-rich member stratigraphically above Fe/Mg-phyllosilicate-rich member exposed along the upper parts of a pit wall south of Coprates Chasma [*Le Deit et al.*, 2010a, 2010b]. Portion of HiRISE IRB color image PSP_009143_1645 (image center: −15.07°N, 58.23°W).

impact craters, submitted to *Icarus*, 2012]. Formation #1 has classically been interpreted as Fe/Mg-phyllosilicate-rich material excavated by impacts [e.g., *Mustard et al.*, 2008; *Barnhart and Nimmo*, 2011]. Alternatively, recent studies suggest that some Fe/Mg-phyllosilicate-rich material may have formed by impact-induced hydrothermalism, as has been proposed in Toro Crater (northern edge of Syrtis Major) [*Schwenzer and Kring*, 2009a; *Marzo et al.*, 2010].

[4] Formation #2, for which we suggest the collective name "Valley-Fill Phyllosilicates," consists of subhorizontally layered light-toned materials of various thicknesses, visible on valley floors, in deltas and in depressions, such as Uzboi Vallis [*Grant et al.*, 2010], Holden Crater, Eberswalde Crater [*Pondrelli et al.*, 2008], Ritchey Crater [*Milliken*, 2007], and Shalbatana Vallis [*Le Deit et al.*, 2010b; *Wintzer et al.*, 2011], both on Noachian and Hesperian-aged terrains. Formation #2 is generally interpreted as sedimentary infills deposited during the Noachian and Hesperian times in fluvial channels and standing bodies of water. The phyllosilicates of this formation may have formed by aqueous alteration or diagenesis, either in situ or elsewhere on the plateau before they have been eroded and transported to their current locations [*Grant et al.*, 2010].

[5] Formation #3, for which we suggest the collective name "Chasma Phyllosilicates," consists of massive to blocky material exposed at depth in chasma walls of Valles Marineris [*Murchie et al.*, 2009a; *Roach et al.*, 2010; *Flahaut et al.*, 2012]. Formation #3 is generally interpreted as Fe/Mg-phyllosilicate-rich material formed during the Noachian Epoch by hydrothermal alteration in the cooling crust,

impact-induced hydrothermalism and/or burial metamorphism [*Murchie et al.*, 2009a]. They may also correspond to pedogenic phyllosilicates that were buried by younger lavas.

[6] In this article, we focus on Formation #4, for which we suggest the collective name "Plateau Phyllosilicates" because, as we shall argue, it extensively covers Noachian plateaus around Valles Marineris. This formation includes Fe/Mg-phyllosilicte-rich material exposed along crater rims and valley walls in Noachis Terra [*Wray et al.*, 2009; *Buczkowski et al.*, 2010; *Buczkowski and Seelos*, 2010] and along the upper parts of Coprates Chasma (Figure 1b) [*Murchie et al.*, 2009a]. It also includes Al-phyllosilicate-rich material resting on Fe/Mg-phyllosilicate-rich material exposed along the upper parts of the walls of a pit south of Coprates Chasma (Figure 1b) [*Murchie et al.*, 2009a; *Le Deit et al.*, 2010a, 2010b].

[7] We describe here several dozen new exposures of Al-rich and Fe/Mg-rich materials belonging to this formation on the plateaus and in the upper walls of Valles Marineris between 40°S and 5°N in latitude, and 70°W and 30°W in longitude (Figure 1). This region includes East Thaumasia Planum, northwest Margaritifer Terra, Ophir Planum and South Lunae Planum.

[8] Similar Plateau Phyllosilicates, comprising Al-phyllosilicate-rich material resting on Fe/Mg-phyllosilicate-rich material, are exposed in Mawrth Vallis [*Loizeau et al.*, 2010; *Wray et al.*, 2008; *Bishop et al.*, 2008a; *McKeown et al.*, 2009; *Noe Dobrea et al.*, 2010], in Nili Fossae [*Ehlmann et al.*, 2009], in northeast Noachis Terra [*Wray et al.*, 2009] and along the upper parts of the walls of a pit

south of Coprates Chasma (Figure 1b) [*Murchie et al.*, 2009a, *Le Deit et al.*, 2010a, 2010b].

[9] We analyze here the morphology, spatial distribution, internal stratigraphy, and mineralogical composition of the Plateau Phyllosilicates around Valles Marineris and discuss their formation processes. We also examine the stratigraphical relationships of this phyllosilicate-rich formation with other sedimentary formations in order to better constrain the geological history of the region and the evolution of the geochemical and climatic conditions through time.

2. Data and Methods

2.1. Hyperspectral Imaging Data

[10] We used Compact Reconnaissance Imaging Spectrometer for Mars (CRISM) hyperspectral data in the near-infrared wavelengths to determine the occurrence or the absence of phyllosilicate-rich materials, and to characterize their mineralogical composition. In the targeted hyperspectral mode, the CRISM instrument provides 10 km × 10 km images with a spatial resolution of 18 m/pixel, and with a 544-channels spectrum between 0.362 μm and 3.92 μm for each pixel [*Murchie et al.*, 2007, 2009b]. We analyzed 90 CRISM targeted observations available in the region using the CRISM Analysis tool (CAT) developed for the ENVI software [*Morgan et al.*, 2009]. CRISM observations were corrected from atmospheric effects using the procedure of *McGuire et al.* [2009]. Noise was reduced using the CIRRUS destriping and despiking function of the CAT [*Parente*, 2008]. The Flatten Summary Product function of the CAT enabled us to reduce the "spectral smile" [*Murchie et al.*, 2007] in the mineralogical maps, which were computed using the spectral parameter summary products described in *Pelkey et al.* [2007].

[11] Spectra of Fe/Mg-rich phyllosilicates and Al-rich phyllosilicates display diagnostic absorption bands at 1.9 μm and 2.3 μm, and 1.9 μm and 2.2 μm respectively [*Clark et al.*, 1990; *Poulet et al.*, 2005]. The Fe/Mg-rich phyllosilicates were mapped using the spectral parameters D2300, calculating the 2.3 μm drop and BD1900R, calculating the 1.9 μm band depth. The Al-rich phyllosilicates were mapped using the spectral parameters BD2200, calculating the 2.2 μm band depth, and BD1900R.

[12] We calculated averaged spectra of regions encompassing tens of pixels, which were selected according to the characteristics of their spectral signatures. The selection of these regions of interest was made by the study of band depth maps. We divided the averaged spectra by spectra of neutral, homogeneous, and often dusty regions extracted from the same columns of the same hyperspectral image. This ratio method reduces the noise inherent to the data and emphasizes the absorption bands, reducing environmental effects such as dust and atmospheric residuals. It provides ratioed spectra, which can be compared to spectra of pure minerals measured in the laboratory.

2.2. Imaging Data

[13] We analyzed more than one hundred images from the High Resolution Imaging Science Experiment (HiRISE, 25–32 cm/pixel) [*McEwen et al.*, 2007]. For each observation, we investigated the occurrence of materials belonging to Plateau Phyllosilicates formation first identified in CRISM data on plateaus, valley walls, chasma walls and crater rims. We analyzed their morphology and color variations on HiRISE Red and IRB false color images. These IRB false color images correspond to color compositions of near infrared (0.8 to 1 μm, red channel), red (0.57 to 0.83 μm, green channel), and blue-green (0.4 to 0.6 μm, blue channel) images that can be used for extrapolating CRISM results to smaller spatial scales (A. S. McEwen and E. Eliason, Information for Scientific Users of HiRISE Color Products, University of Arizona, 2007, http://hirise.lpl.arizona.edu/pdf/color-products.pdf). The combined analysis of CRISM and HiRISE data allowed us to identify diagnostic morphological features for the phyllosilicate-rich materials. In some instances, CRISM data were not available in areas where HiRISE images indicate the probable presence of phyllosilicate-rich materials.

[14] The phyllosilicate-rich materials identified with CRISM data are visible on nadir panchromatic images of the High Resolution Stereographic Camera (HRSC, 12.5–30 m/pixel) [*Neukum and Jaumann*, 2004] and the Context Camera (CTX, 6 m/pixel) [*Malin et al.*, 2007] These two data sets provide a nearly full coverage of the studied region that allowed us to extend geological mapping of the phyllosilicate-rich formation to a regional scale (Figure 2).

[15] We excluded phyllosilicate-rich materials located in large impact craters and along complex crater rims (i.e., Ritchey Crater). These sites correspond to complex geological contexts in which the phyllosilicate-rich materials may

Figure 2. Spatial distribution of Plateau Phyllosilicates in the Valles Marineris region. (a) Regional map encompassing the whole study area. The phyllosilicate-rich materials identified by CRISM data are indicated by squares and are reported over the global geological map of Mars [*Scott and Tanaka*, 1986] (cs, impact crater material; Nplr, plateau sequence, ridged unit; Nplh, plateau sequence, hilly unit; Npld, plateau sequence, dissected unit; Npl$_2$, plateau sequence, subdued cratered unit; Npl$_1$, plateau sequence, cratered unit; Nf, highly deformed terrain materials, older fractured material; Hvl, Valles Marineris interior deposits, layered material; Hr, ridged plains material; Hpl$_3$, plateau sequence, smooth unit; Hf, younger fractured material; Hcht, older chaotic material; Hch, older channel material; HNu, undivided material; Avf, Valles Marineris interior deposits, floor material). Blue squares indicate materials for which the corresponding spectra exhibit hydration features at 1.9 μm but lack additional diagnostic features. Light-toned materials that have the characteristic morphologies of the Plateau Phyllosilicates are indicated by circles. The distinction between Al- and Fe/Mg-phyllosilicate-rich materials cannot be made at the scale of this map. The Layered Deposits (LDs) correspond to light-toned material locally covering the plateaus around Valles Marineris [*Le Deit et al.*, 2010c] and are locally enriched in opaline silica and hydroxylated ferric sulfates [*Bishop et al.*, 2009; *Le Deit et al.*, 2010c]. Locations of Figures 2b and 2c are indicated by white boxes. Locations of Figures 4–6, 8–13, and 15 are shown by bracketed numbers. (b) Close-up view of Ophir Planum. The Plateau Phyllosilicates mapped with HRSC panchromatic nadir images are displayed on a mosaic of THEMIS IR daytime images. (c) Close-up view of Thaumasia Planum. Plateau Phyllosilicates are shown on the global geological map of Mars [*Scott and Tanaka*, 1986].
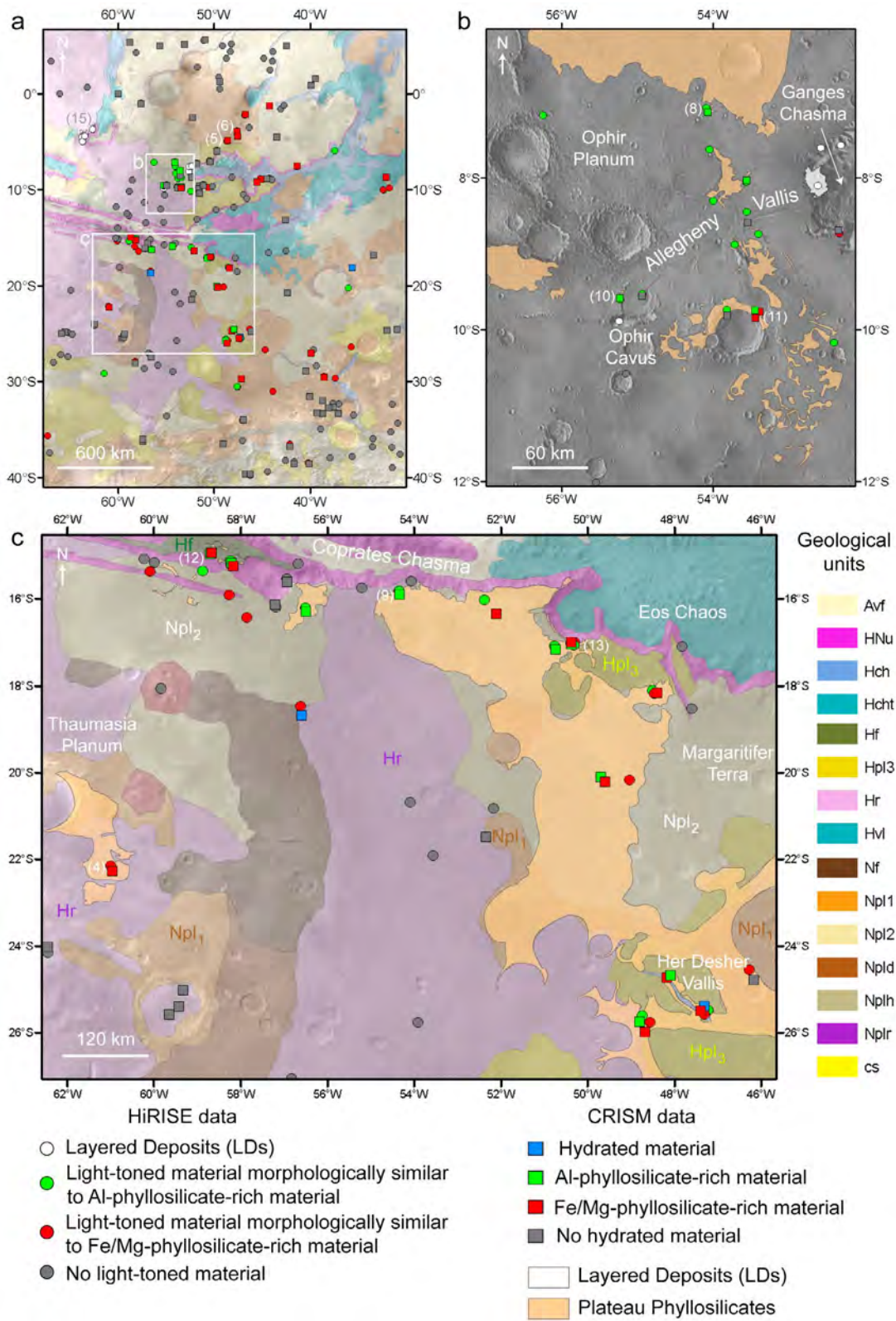
Figure 2

Table 1. List of CRISM Observations Analyzed Where phyllosilicates and Hydrated Minerals are Detected[a]

CRISM Observation ID[b]	Location		Surface Geological Unit	Geological Context	Mineralogical Composition
	Latitude (°N)	Longitude (°W)			
FRT A865	−8.91	−45.11	Npl_2[c]	Crater rim along Ganges Chasma	Fe/Mg-rich phyllosilicates
FRT 949A (6)	−3.92	−47.59	Npl_1	Shalbatana Vallis wall	Fe/Mg-rich phyllosilicates
FRT BE32	−4.41	−47.56	Npl_1	Pit wall	Fe/Mg-rich phyllosilicates
FRT 815B	−1.27	−44.21	Npl_2	Ravi Chaos wall	Fe/Mg-rich phyllosilicates
FRT C875	−29.44	−38.54	Npl_1	Nirgal Vallis wall	Fe/Mg-rich phyllosilicates
HRS A8D3 (4)	−22.25	−60.97	Npl_2[d]	Plateau	Fe/Mg-rich phyllosilicates
FRT AA4A	−29.75	−47.20	Npl_1	Crater rim	Fe/Mg-rich phyllosilicates
HRL AB96	−27.21	−39.88	Npl_2	Crater rim	Fe/Mg-rich phyllosilicates
FRT 11728	−18.16	−48.43	Npl_2	Plateau and pit wall	Fe/Mg-rich phyllosilicates
FRT 132AD	−16.43	−52.00	Npl_2	Plateau	Fe/Mg-rich phyllosilicates
HRL BF2B (5)	−4.91	−48.58	Npl_1	Plateau and crater rim	Fe/Mg-rich phyllosilicates
FRT 5461	−8.70	−32.12	Npl_2	Chaos rim	Fe/Mg-rich phyllosilicates
HRL 7FF1	−7.58	−41.35	Npl_2	Crater rim along Capri Chasma	Fe/Mg-rich phyllosilicates
FRT 8EBF	−2.15	−46.74	Npl_1	Crater rim	Fe/Mg-rich phyllosilicates
FRT B44D (10)	−9.60	−55.20	Npl_1	Allegheny Vallis wall	Al-rich phyllosilicates
FRT B092 (8)	−7.10	−54.07	Npl_2	Plateau	Al-rich phyllosilicates
HRL BADC	−8.06	−53.55	Npl_2	Plateau	Al-rich phyllosilicates
FRT A51A (9)	−15.81	−54.33	Npl_2	Plateau	Al-rich phyllosilicates
HRL 67F1	−17.10	−50.74	Npl_2	Plateau	Al-rich phyllosilicates
HRL BDBB	−16.23	−56.49	Npl_2	Plateau	Al-rich phyllosilicates
HRL 80CB (11)	−9.84	−53.42	Npl_2	Plateau, valley wall, and crater rim	Al-rich and Fe/Mg-rich phyllosilicates
FRT B278	−9.15	−45.54	Npl_2[c]	Ganges Chaos wall	Al-rich and Fe/Mg-rich phyllosilicates
FRT B6C5	−15.15	−58.19	Npl_2	Plateau and Coprates Chasma wall	Al-rich and Fe/Mg-rich phyllosilicates
HRL BECE (12)	−14.95	−58.66	Npl_2	Plateau and Coprates Chasma wall	Al-rich and Fe/Mg-rich phyllosilicates
FRT B23E	−20.15	−49.61	Npl_2	Plateau	Al-rich and Fe/Mg-rich phyllosilicates
FRT D23E (13)	−17.05	−50.36	Npl_2	Plateau and Eos Chasma wall	Al-rich and Fe/Mg-rich phyllosilicates
FRT 8E5D	−25.71	−48.64	Hpl_3	Valley wall and crater rim	Al-rich and Fe/Mg-rich phyllosilicates
FRT 137AD	−24.75	−48.20	Hpl_3	Her Desher Vallis wall	Al-rich and Fe/Mg-rich phyllosilicates
FRT B58A	−18.38	−56.63	Npl_2	Plateau	Hydrated minerals
HRS 84F4	−18.18	−35.67	Npl_1	Crater Rim	Hydrated minerals
HRL 9B61	−25.48	−47.24	Hpl_3	Her Desher Vallis wall	Hydrated minerals and Fe/Mg-rich phyllosilicates

[a]The corresponding locations, geological units, and geological contexts are indicated.
[b]Number in parentheses refers to figure numbers in this paper.
[c]Mapped as Hpl_3 on the map of *Scott and Tanaka* [1986], and as Npl_2 on that of *Witbeck et al.* [1991].
[d]Mapped as Hr on the map of *Scott and Tanaka* [1986], and as Npl_2 on that of *Dohm et al.* [2001].

have formed in response to a number of processes (i.e., excavated bedrock, post-impact induced hydrothermalism, sedimentary deposition, in situ alteration), that may be distinct from those responsible for the development of Plateau Phyllosilicates.

[16] Finally, we examined the location of the Plateau Phyllosilicates with respect to the geological maps of *Scott and Tanaka* [1986], *Witbeck et al.* [1991], and *Dohm et al.* [2001] in order to obtain stratigraphic constraints on their age of formation. The spatial distribution, morphology, internal stratigraphy and mineralogical composition of the Plateau Phyllosilicates are described hereafter.

3. Spatial Distribution and Geological Context

[17] The occurrence or absence of phyllosilicate-rich materials is indicated by squares on Figure 2 for each CRISM image. Light-toned materials that have the morphology and the color characteristic of Plateau Phyllosilicates in HiRISE images are indicated by circles. In Table 1 all locations where we detected phyllosilicate-rich materials using CRISM data and their corresponding geological context are reported.

[18] Exposures of phyllosilicate-rich materials are widespread in the study region. Hundreds of outcrops consisting of light-toned material containing phyllosilicates are scattered over an area wider than 2800×2300 km. The number of phyllosilicate-rich outcrops may be under-estimated due to their small size and high noise levels in CRISM data. The estimated minimum surface area of the corresponding phyllosilicate-rich formation is $\sim$197,000 km^2. This is much larger than the surface area covered by other hydrated formations observed on the plateau such as the layered deposits located close to Ganges Chasma ($\sim$300 km^2) [*Le Deit et al.*, 2010c]. Topographic data from the gridded 128 pixels/deg Mars Orbiter Laser Altimeter (MOLA) DEM and from the MOLA PEDR single tracks [*Smith et al.*, 2001] indicate that the "Plateau Phyllosilicates" formation is tens of meters thick and is located at elevations ranging between −2798 m and 3363 m. It is fairly well exposed close to Shalbatana Vallis (Figure 2a), west of Ganges Chasma (Figure 2b), and south of Coprates Chasma and Eos Chaos up to Her Desher Vallis and Nirgal Vallis (Figure 2c). All exposures are located in Noachian units, mainly the Npl_1 unit (plateau sequence, cratered unit), and the younger Npl_2 unit (plateau sequence,
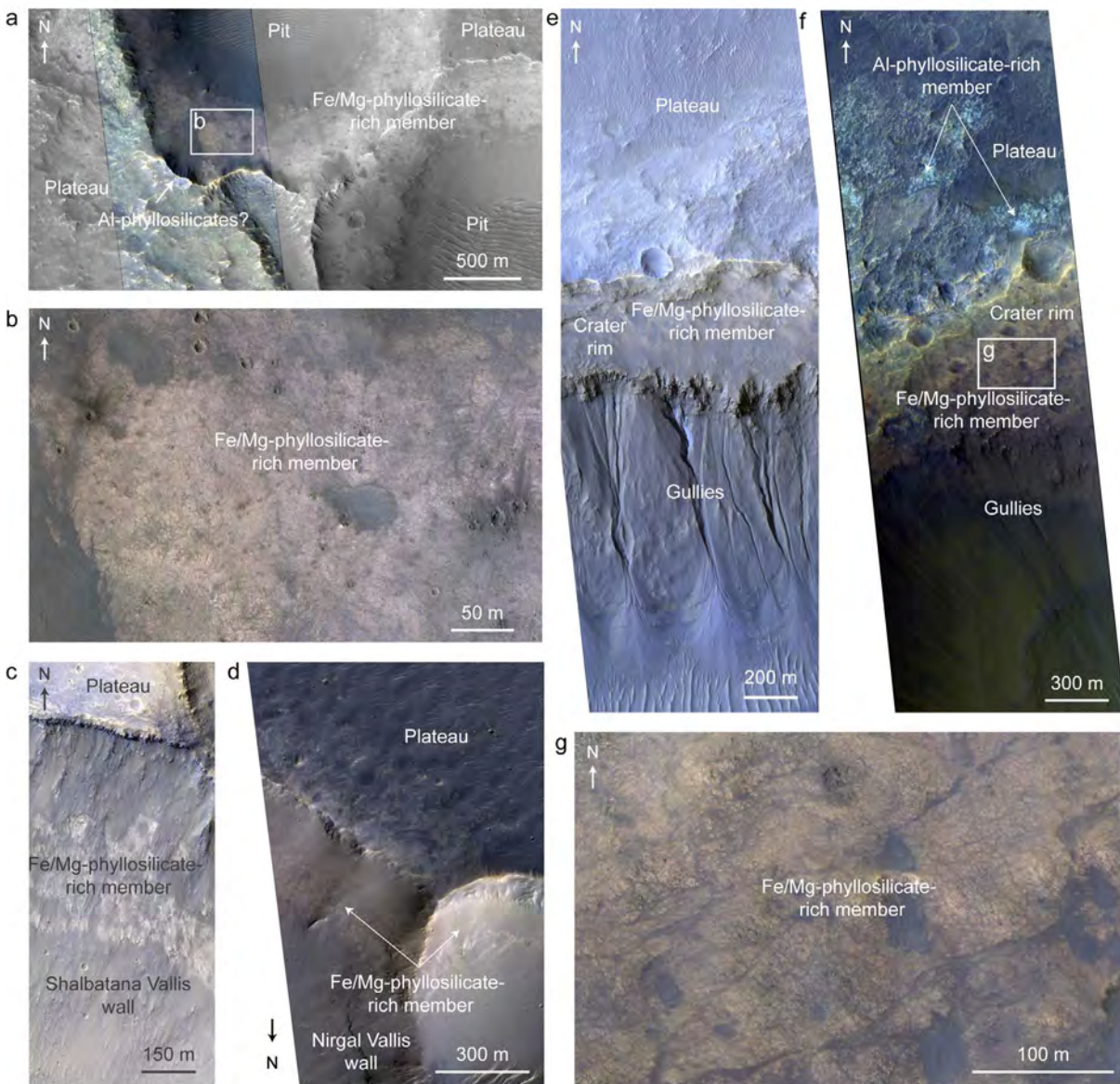
Figure 3. Morphology of the Fe/Mg-member. (a) Portion of HiRISE Red image (ESP_012215_1615) overlain by the corresponding IRB color image showing the Fe/Mg-member cropping out along pit walls south of Eos Chaos (image center: −18.1°N, 48.4°W). Outcrops on the plateau are locally morphologically similar to the Al-member but Al-phyllosilicates are not clearly identified with CRISM data. Location of Figure 3b is indicated. (b) Close-up view of Figure 3a showing Fe/Mg-member, which is typically reddish on HiRISE IRB color images, and does not displays well defined layers. (c) Light-toned exposure of the Fe/Mg-member along the upper parts of Shalbatana Vallis walls. Portion of HiRISE IRB color image PSP_009459_1755 (image center: −4.4°N, 47.6°W). (d) Upper parts of Nirgal Vallis walls showing the Fe/Mg-member. Portion of HiRISE IRB color image ESP_016764_1505 (image center: −29.4°N, 38.7°W). (e) Fe/Mg-member exposed on the upper parts of a crater wall above a series of more competent layers. The mineralogical composition of the Fe/Mg-member has not been studied with CRISM analysis (absence of data) but its identification is suggested by its morphological characteristics (see section 2.2 for more details). Gullies are carved in the bottom parts of the crater wall. Portion of HiRISE IRB color image ESP_011727_1490 (image center: −30.9°N, 43.9°W). (f) Fe/Mg- and Al-members exposed on the crater rims and on the surrounding plateau respectively. The mineralogical composition of the light-toned materials has not been studied with CRISM analysis (absence of data) but their morphological characteristics suggest that they correspond to Plateau Phyllosilicates (see section 2.2 for more detail). Gullies are carved in the bottom parts of the crater rim. Portion of HiRISE IRB color image ESP_012426_1490 (image center: −30.6°N, 47.5°W). (g) Close-up view of Figure 3f showing the Fe/Mg-member. It displays small polygonal fractures and no layers.
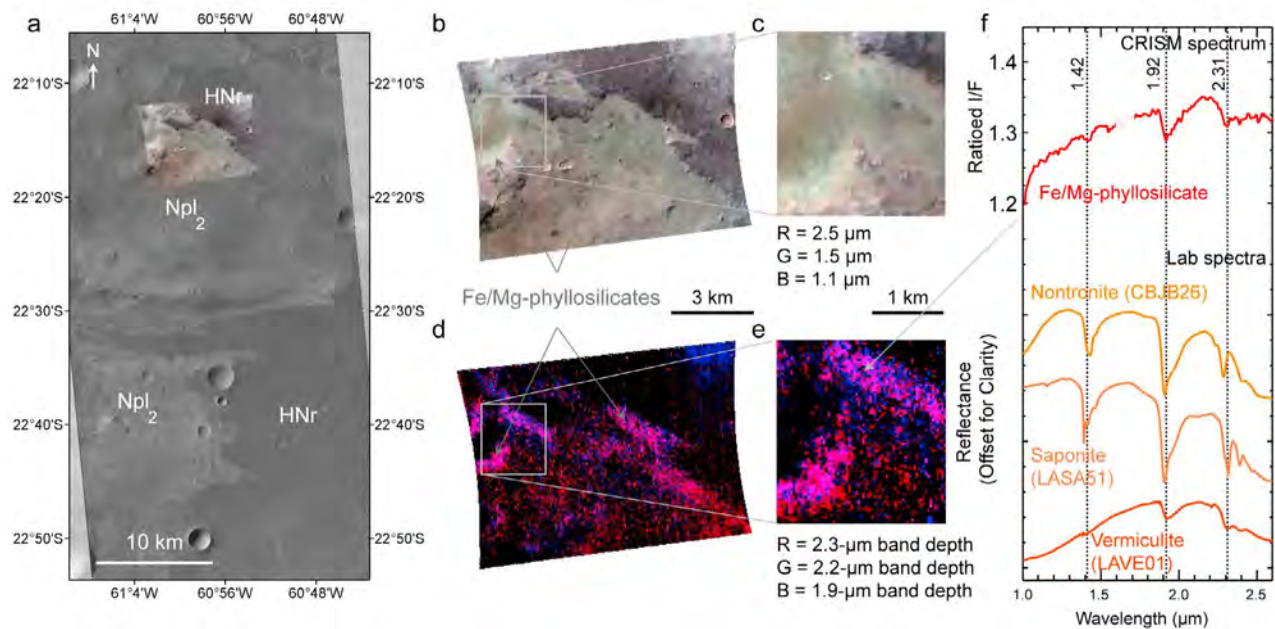
Figure 4. Spectral properties and morphology of the Fe/Mg-phyllosilicate-rich member cropping out on plateau in East Thaumasia Planum. (a) The Fe/Mg-member is exposed on the Noachian unit Npl_2, which is partly buried by the Late Noachian/Early Hesperian unit HNr (Younger ridged plains material). Subset of CTX image B02_010409_1577 overlain by CRISM image HRS A8D3. (b) False color image of the CRISM observation HRS A8D3. (c) Close-up view of Figure 4b. (d) Band depth map of the same observation (red, D2300; green, BD2200; blue, BD1900R). Stretched values: red, 0.001–0.016; green, 0.001–0.195; blue, 0.001–0.018. Pink tones indicate occurrence of Fe/Mg-phyllosilicates, and blue tones of hydrated phases. (e) Close-up view of Figure 4d. (f) CRISM spectrum of Fe/Mg-phyllosilicate (average of 13 pixels divided by an average of 25 pixels of a neutral region) compared to laboratory spectra (RELAB library spectra). Locations of the averaged pixels are indicated by arrows toward Figure 4e.

subdued cratered unit; Figure 2a). The Npl_1 unit is interpreted as volcanic materials and impact breccia that were emplaced throughout the region during the heavy meteorite bombardment and the Npl_2 unit as dominantly lava flows and eolian material [*Witbeck et al.*, 1991]. In a few instances, the phyllosilicate-rich formation is located within the geographical extent of Hesperian units (e.g., Hpl_3, plateau sequence, smooth unit; HNu, undivided material) on the regional maps of *Scott and Tanaka* [1986] (Figure 2c) and *Witbeck et al.* [1991]. But high-resolution HiRISE images and the regional map of *Dohm et al.* [2001] reveal that the phyllosilicate-rich materials actually correspond to small outcrops of Noachian terrains scattered within these Hesperian units (Figure 4).

4. Internal Stratigraphy

[19] As we shall now discuss, the "Plateau Phyllosilicates" formation comprises a Fe/Mg-phyllosilicate-rich lower member and an Al-phyllosilicate-rich upper member.

4.1. Fe/Mg-Member

[20] The Fe/Mg-phyllosilicate-rich member is light-toned compared to dust and often appears reddish on HiRISE IRB color images (Figures 3b, 3d, 3f, and 3g). This member is massive (Figures 4b, 4c and 5g) or polygonally fractured, (Figures 3b and 3g), similar to phyllosilicate-rich materials observed in Mawrth Vallis [e.g., *Bishop et al.*, 2008a;

McKeown et al., 2009; *Loizeau et al.*, 2010]. The polygons are generally small (meter scale at HiRISE resolution). These morphological characteristics are variable but it makes the Fe/Mg-member clearly identifiable on HiRISE images.

[21] The Fe/Mg-phyllosilicate-rich member rests on top of the Noachian basement, either as relatively flat exposures on plateaus (Ophir Planum, Thaumasia Planum, Margaritifer Terra; Figures 2, 4, 5, and 13), or along the upper parts of scarps including valley walls (Shalbatana Vallis, Her Desher Vallis, Nirgal Vallis; Figures 6 and 11), chasma walls (Ganges and Coprates chasmata, Eos Chaos; Figure 13), pit walls and small impact crater rims (Figures 5 and 12 and Table 1). In some instances, the Fe/Mg-member is located along the upper part of impact crater rims above gullies. For instance, in Figures 3e–3g, the Fe/Mg-member crops out on a bench bounded by the very near surface and a layer of competent rock carved by gullies.

[22] Three characteristic sites of the Fe/Mg-member are displayed in Figures 4 to 6. In Figure 4, a site where the Fe/Mg-member is exposed on the plateau in East Thaumasia Planum is shown. The Fe/Mg-member crops out above the light-toned unit Npl_2 (Figures 4a–4e). It is locally buried by the Late Noachian/Early Hesperian unit HNr, which corresponds to older ridged plains material interpreted to be lava flows [*Dohm et al.*, 2001]. The Fe/Mg-phyllosilicates appear pink in the band depth map of the CRISM observation (Figures 4d–4e) and cyan in the false color image of the same observation (Figures 4b–4c). Many exposures of the
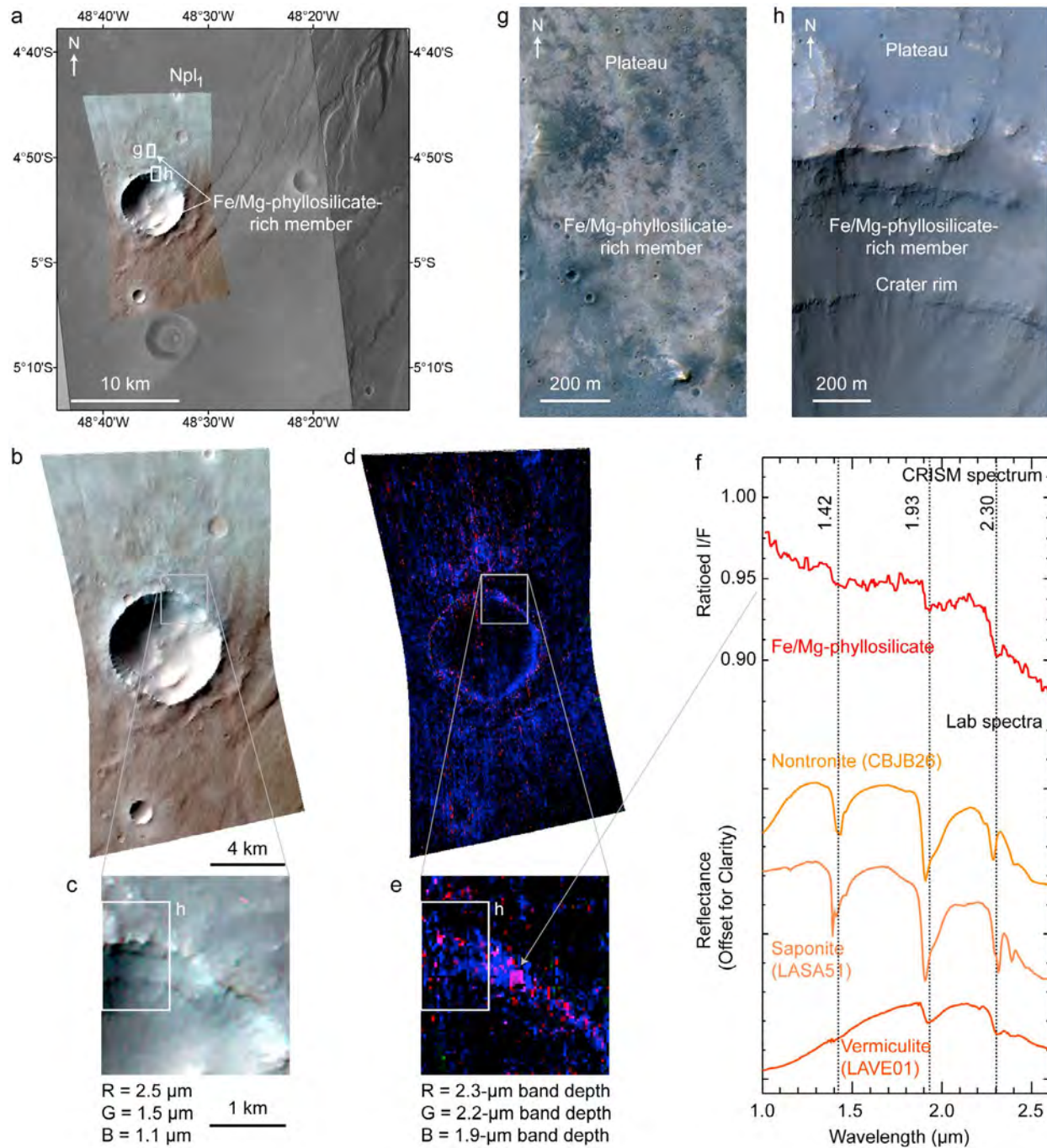
Figure 5. Spectral properties and morphology of the Fe/Mg-phyllosilicate-rich member cropping out on the plateau north of Ganges Chasma. (a) The Fe/Mg-member is exposed on the plateau and on the upper part of an impact crater rim. Subsets of CTX image P08_0004251_1751 and HRSC nadir image 7201 overlain by CRISM image HRL BF2B. Locations of Figures 5g and 5h are indicated. (b) False color image of the CRISM observation HRL BF2B. (c) Close-up view of Figure 5b. Location of Figure 5h is indicated. (d) Band depth map of the same observation (red, D2300; green, BD2200; blue, BD1900R). Stretched values: red, 0.001–0.017; green, 0.001–0.195; blue, 0.001–0.014. Pink tones indicate occurrence of Fe/Mg-phyllosilicates, and blue tones of hydrated phases. (e) Close-up view of Figure 5d. Location of Figure 5h is indicated. (f) CRISM spectrum of Fe/Mg-phyllosilicate (average of 23 pixels divided by an average of 16 pixels of a neutral region) compared to laboratory spectra (RELAB library spectra). Locations of the averaged pixels are indicated by arrows toward Figure 5e. (g) Portion of HiRISE IRB color image ESP_017028_1750 showing a close-up view of the Fe/Mg-member on the plateau (image center: −4.82°N, 48.59°W). (h) Portion of the same HiRISE image showing a close-up view of the Fe/Mg-member along the crater rim (image center: −4.86°N, 48.58°W).
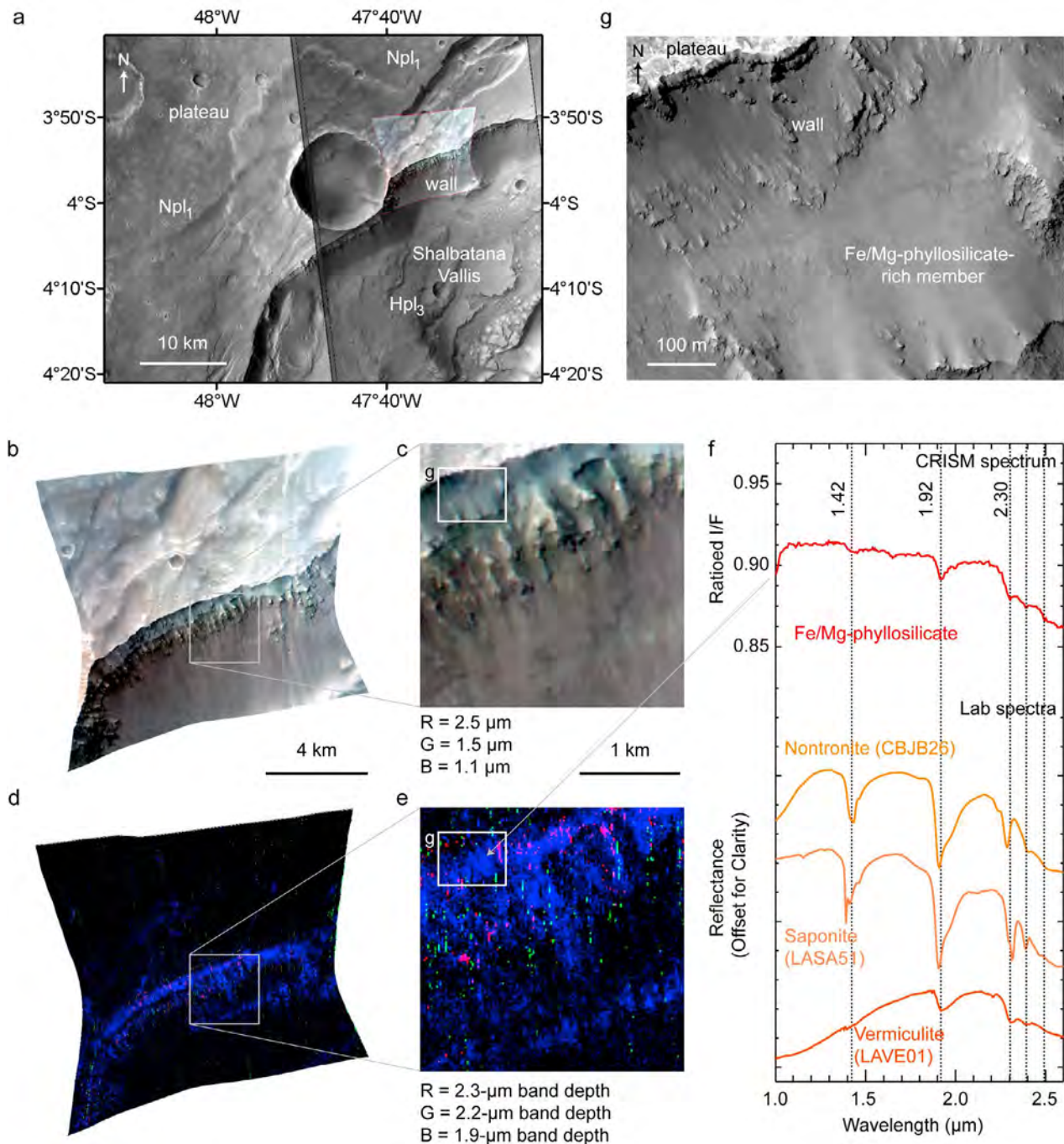
Figure 6. Spectral properties and morphology of the Fe/Mg-phyllosilicate-rich member cropping out on the upper part of the wall of Shalbatana Vallis. (a) Subsets of CTX images P06_0003262_1753 and P15_006809_1740 overlain by CRISM image FRT 949A. (b) False color image of the CRISM observation FRT 949A. (c) Close-up view of Figure 6b. Location of Figure 6g is indicated. (d) Band depth map of the same observation (red, D2300; green, BD2200; blue, BD1900R). Stretched values: red, 0.001–0.005; green, 0.002–0.008; blue, 0.001–0.011. Pink tones indicate occurrence of Fe/Mg-phyllosilicates, and blue tones of hydrated phases. (e) Close-up view of Figure 6d. Location of Figure 6g is indicated. (f) CRISM spectrum of Fe/Mg-phyllosilicate (average of 21 pixels divided by an average of 16 pixels of a neutral region) compared to laboratory spectra (RELAB library spectra). Locations of the averaged pixels are indicated by arrows toward Figure 6e. (g) Portion of HiRISE Red image PSP_006809_1760 showing a close-up view of the Fe/Mg-member (image center: −3.92°N, 47.59°W).
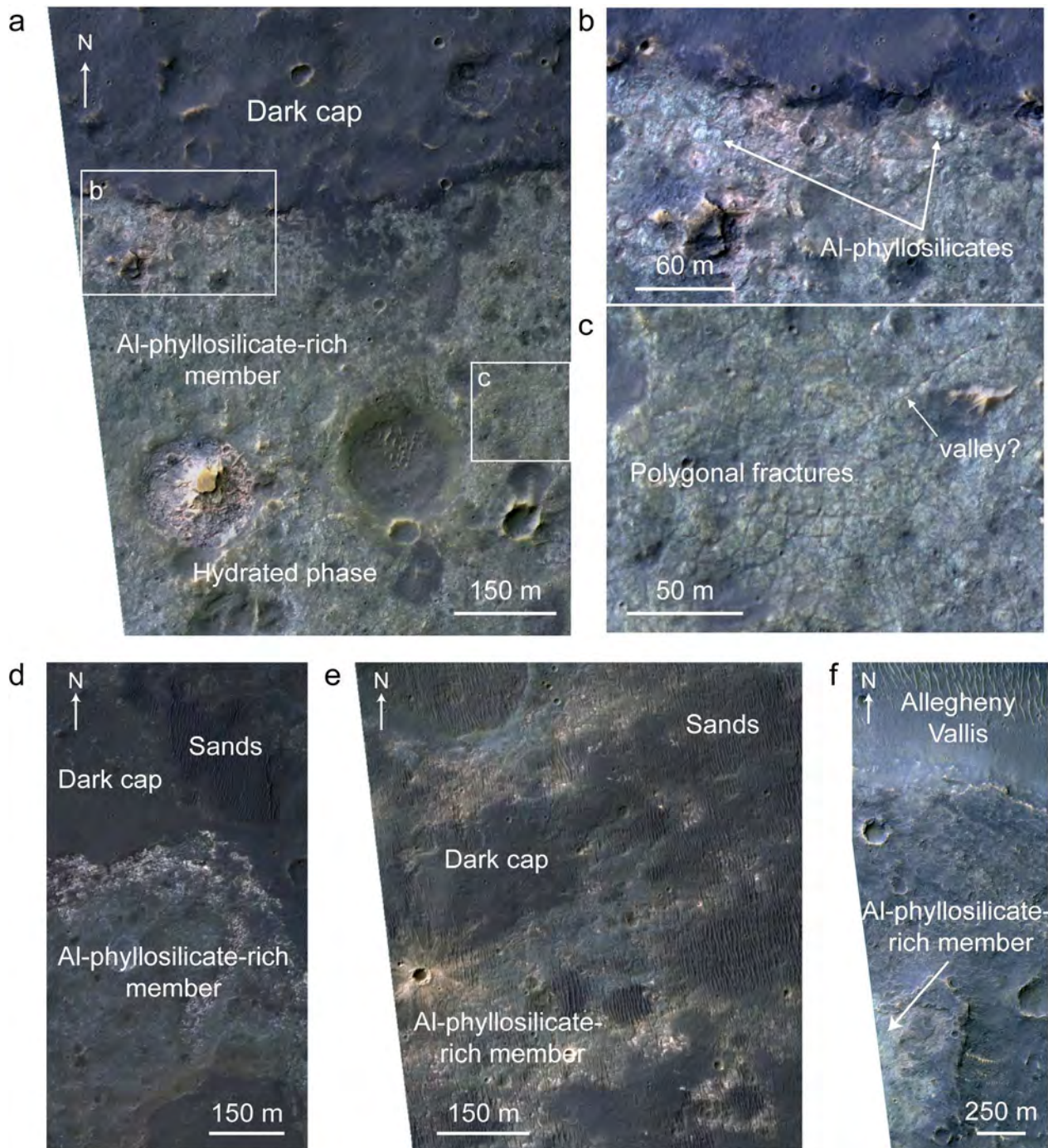
Figure 7. Morphology of the Al-member exposed on plateaus and along valley walls. (a) The Al-member is white, light blue to green on this portion of HIRISE IRB color image PSP_008800_1730 located on Ophir Planum (image center: −7.1°N, 54.12°W). In green tone, the material is hydrated and does not display strong signature of Al-phyllosilicates. Location of Figures 7b and 7c is indicated. (b) Close-up view of Figure 7a showing white-blue outcrops characterized by a strong spectral signature of Al-phyllosilicates. (c) Close-up view of Figure 7a showing the rough texture of the Al-member affected by polygonal fractures, and incised by valleys. (d) Exposure of the Al-member on the plateau south of Coprates Chasma. Portion of HIRISE IRB color image PSP_009143_1645 (image center: −15.1°N, 58.2°W). (e) Extended Al-member covered by isolated exposures of dark cap and sands. Portion of HIRISE IRB color image PSP_009433_1635 (image center: −16.2°N, 56.5°W). (f) Al-member cropping out south of a main bed of Allegheny Vallis. Portion of HIRISE IRB color image PSP_009578_1715 (image center: −8.55°N, 53.56°W).
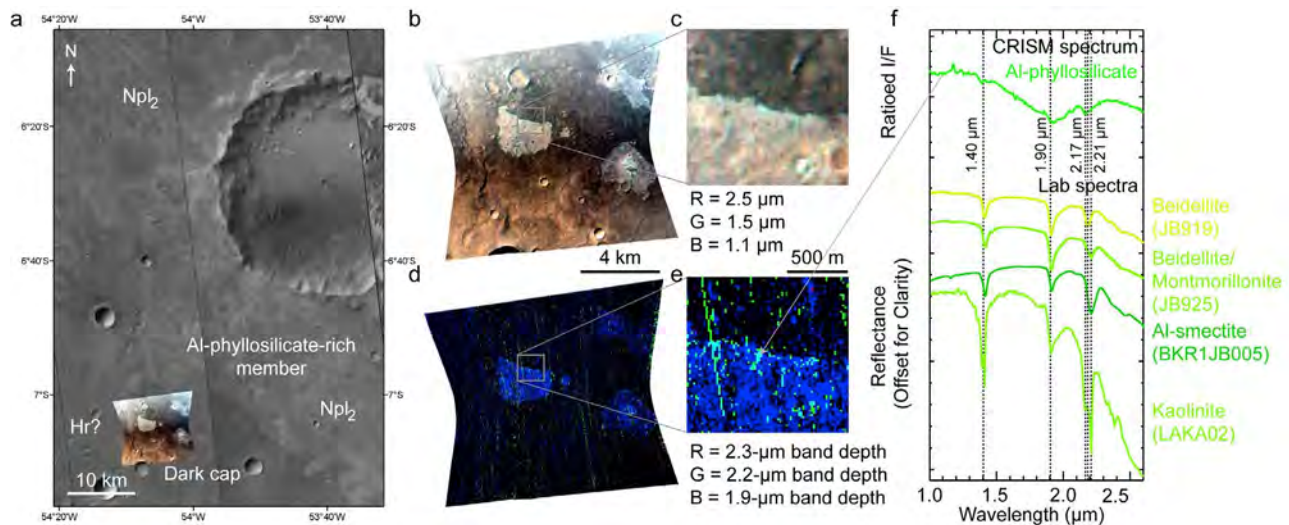
Figure 8. Spectral properties of the Al-phyllosilicate-rich member exposed on Ophir Planum. (a) Exposures of the light-toned Al-member on the Npl_2 unit. The dark cap possibly corresponds to the Hr unit. Portions of CTX images P18_008009_1725 and P20_008800_1732 overlain by CRISM image FRT B092. The corresponding HiRISE image is shown in Figures 3a–3c. (b) False color image of the CRISM observation FRT B092. (c) Close-up view of Figure 8b. (d) Band depth map of the same observation (red, D2300; green, BD2200; blue, BD1900R). Stretched values: red, 0.001–0.022; green, 0.009–0.012; blue, 0.001–0.013. Cyan tones represent occurrences of Al-phyllosilicates, and blue tones represent occurrences of hydrated phases. (e) Close-up view of Figure 8d. (f) CRISM spectrum of Al-phyllosilicate compared to laboratory spectra (RELAB library spectra). Reflectance spectra of beidellite and beidellite/montmorillonite have been measured by *Bishop et al.* [2011]. Location of the averaged pixels is indicated by the arrow toward Figure 8e.

Fe/Mg-member are located close to the lava flow outcrops (Figures 4b–4e).

[23] The next site is an impact crater located on Ophir Planum north of Ganges Chasma (Figure 5). The unit exposed at the surface of the plateau is the cratered unit Npl_1. The Fe/Mg-member (pink in Figures 5d–5e and cyan in Figures 5b–5c) is exposed in the upper part of the impact crater rim (Figure 5h) and on the surrounding plateau (Figure 5g). Fe/Mg-phyllosilicates are not identified in all exposures of light-toned material of the area. Much of this light-toned material is however composed of hydrated minerals (blue in Figures 5d–5e). It is possible that these hydrated minerals include Fe/Mg- phyllosilicates in an amount too small for their diagnostic absorption band at 2.3 μm to be detected. Another possible explanation is that these minerals correspond to a hydrated mineral phase different from Fe/Mg-phyllosilicates.

[24] The Fe/Mg-member also crops out along valley walls. CRISM observation FRT 949A shows that Fe/Mg-phyllosilicates (pink in Figures 6d–6e and cyan in Figures 6b–6c) are located along the upper part of Shalbatana Vallis wall where the Fe/Mg-member corresponds to a massive unit exposed on a gentle slope (Figures 6c, 6e, and 6g).

4.2. Al-Member

[25] Spectra of the Al-phyllosilicate-rich member display absorption bands at $\sim$1.4 μm, $\sim$1.9 μm and at $\sim$2.2 μm. This member is light-toned and appears light-blue to green on HiRISE IRB color images (Figure 7). Green outcrops correspond to hydrated minerals but usually do not display strong

signatures of Al-phyllosilicates (Figures 7a, 7c, and 8), contrary to those appearing light-blue to white (Figures 7a, 7b, and 8). The Al-member locally displays broad polygons (tens of meters wide). It is usually exposed where a dark cap corresponding perhaps to Hesperian lava flows or dark sands has been eroded and removed from the surface. The areas where the Al-phyllosilicate signature is the strongest are usually those located closest to the dark cap outcrops, so they consequently correspond to the freshest exposed areas of the formation.

[26] Like the Fe/Mg-member, the Al-member crops out either as flat exposures on the plateaus (Figures 8–9) or in the upper part of valley walls (Figures 10–11) and chasma walls (Figures 11, 12, and 13 and Table 1).

[27] Typical examples of the Al-member on plateaus are observed on Ophir Planum and south of Coprates Chasma (Figures 8 and 9). In both cases the Al-member outcrops are located on Unit Npl_2 (Figures 8a and 9a) and are locally capped by dark lava flows corresponding to Unit Hr.

[28] The Al-member also crops out along the upper part of valley walls such as in Allegheny Vallis, which originates from Ophir Cavus (Figure 10). The Al-member is exposed on the western side of the valley only, which is located 60 m higher than the eastern side. The Al-member is exposed on the Npl_1 unit and is capped by dark material. No Al-phyllosilicate-rich material is observed on the valley floor.

4.3. Stratigraphic Relationships Between Fe/Mg-Member and Al-Member

[29] At some locations, both the Al-member and the Fe/Mg-member are visible (Figures 11–13). Wherever it is
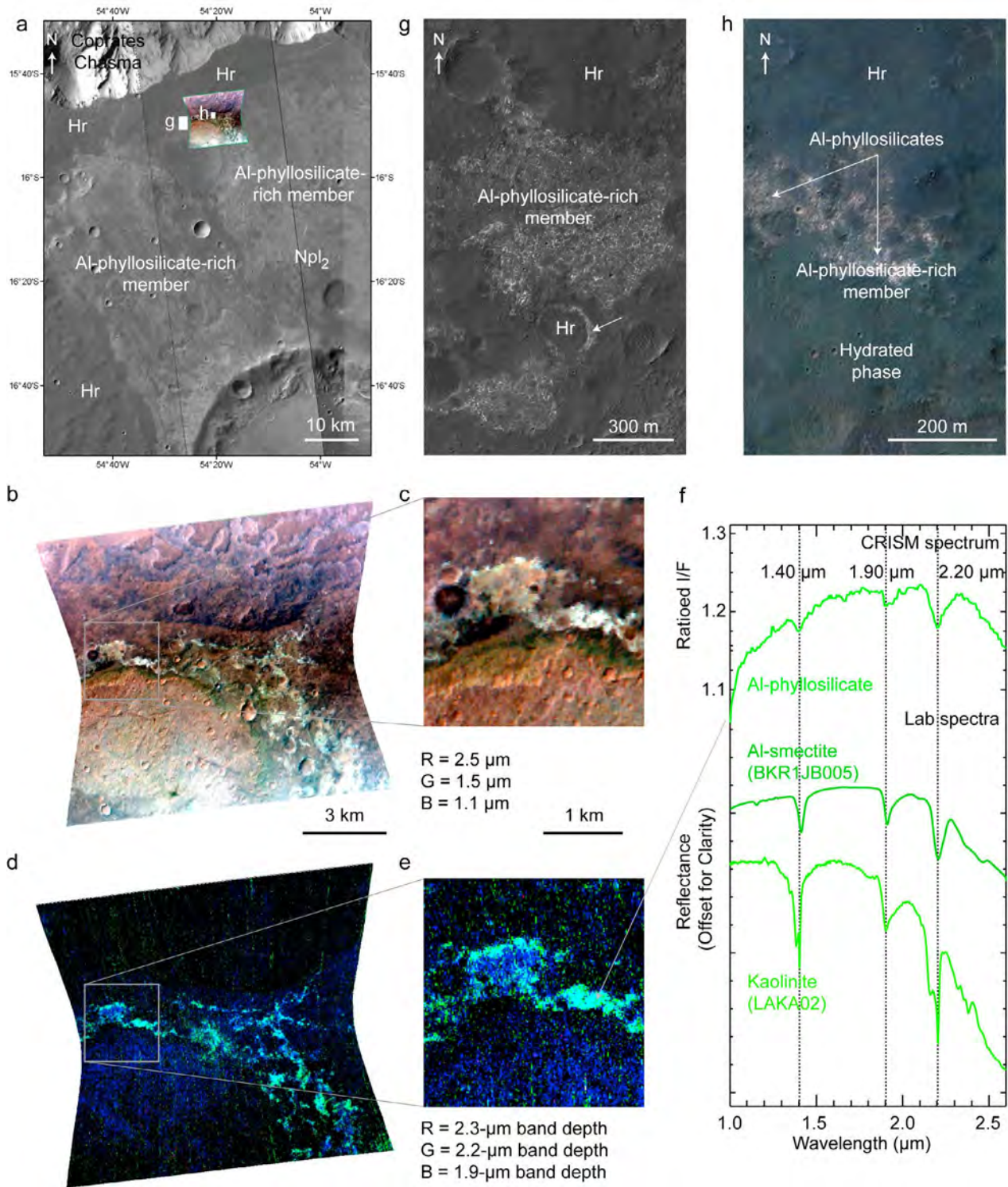
Figure 9

possible to determine their stratigraphical relationships, the Al-member is located stratigraphically above the Fe/Mg-member (Figure 1b). On Figure 11 the rim of an impact crater 40 km in diameter is incised by a valley ~2 km wide, ~5 km long, and up to ~400 m deep. A fan-shaped deposit is located on the crater floor at the outlet of the valley. Along the upper part of the valley wall, the ~30 m thick Fe/Mg-member is exposed. A very thin layer of Al-phyllosilicate-rich material is visible on HiRISE and CRISM images (Figures 11e–11g). This material is located topographically and stratigraphically above the Fe/Mg-member. Some Fe/Mg-phyllosilicates also occur at the surface of the fan-shaped deposit. These are "Valley-Fill Phyllosilicates," as defined in the introduction of this article. Pits located south of Coprates Chasma are shown in Figure 12. The Al-member crops out along the upper part of pit rims and on the surrounding plateau on unit Npl_2. The Fe/Mg-member is exposed along pit rims, below the Al-member. We observe the same stratigraphical relationships along Eos Chasma walls (Figure 13).

5. Mineralogical Composition

[30] The analysis of CRISM data provides constraints on the nature of the phyllosilicates detected in the region. The Fe/Mg-phyllosilicates spectra display absorption bands at ~1.42 μm, ~1.92 μm and a broad one at ~2.3 μm. From comparisons with laboratory spectra, several species of clays can fit the positions and shapes of these absorption bands. These include Fe/Mg-smectites (e.g., nontronite, saponite) and vermiculite (Figures 4–6 and 11–13). This is in agreement with *Buczkowski and Seelos* [2010] who showed that the phyllosilicates located along Her Descher Vallis and Nirgal Vallis may correspond to a mixture of nontronite and saponite, or to an intermediate phase smectite. These authors also proposed that the phyllosilicates could be a mixed layered chlorite/smectite. However, no chlorite has been detected in our study area. Hence, the Fe/Mg-phyllosilicates may rather correspond to a mixture of Fe/Mg-smectites and vermiculite. The Al-phyllosilicate spectral absorption bands are located at ~1.4 μm, ~1.9 μm and ~2.2 μm. Several clay minerals are consistent with these spectral characteristics. They include Al-smectites (e.g., montmorillonite, beidellite) and kaolinites (Figures 8–10 and 11–13). In most analyzed sites, the Al-phyllosilicates spectra display absorption bands at ~1.4 μm, ~1.9 μm and a sharp band at 2.21 μm, which is most consistent with montmorillonite spectra [*Bishop et al.*,

1993]. However, a mixture with other Al-phyllosilicates cannot be ruled out. In the case of the Al-phyllosilicates located on Ophir Planum shown in Figure 8, the corresponding spectra display absorption bands at ~1.4 μm, ~1.9 μm and at 2.18 μm, which are best fitted by beidellite spectra [*Bishop et al.*, 2011]. Along Allegheny Vallis, the Al-phyllosilicates present at the surface could be pure kaolinite or halloysite (hydrated form, *Giese*, 1988), because their spectra have absorption bands at ~1.4 μm, ~1.9 μm and an asymmetric doublet at 2.17 μm and 2.21 μm [*Bishop et al.*, 2008b] (Figure 10f).

6. Formation Processes

[31] Plateau Phyllosilicates rest on the upper Noachian basement made of volcanic materials, impact breccia, and eolian deposits. This formation, up to tens of meters thick, is extensive and is exposed over a surface area of ~197,000 km^2. Sites displaying the two phyllosilicate-rich members show that the Al-phyllosilicate-rich member, composed of Al-smectites and kaolinites, is situated above the Fe/Mg-member, composed of Fe/Mg-smectites and vermiculites. Most outcrops are located in areas where a dark mafic Hesperian unit has been eroded. Several formation processes that could explain these observations are discussed below (Table 2).

6.1. Surface Water Runoff

[32] Many outcrops of the Plateau Phyllosilicates are located along valley systems including Allegheny Vallis, Her Desher Vallis, and Nirgal Vallis (e.g., Figures 2, 6, 7f, and 9). It is tempting to interpret this as indicating deposition of phyllosilicates by water runoff in low-energy fluvial environments. Phyllosilicates may form by aqueous weathering of volcanic basement rocks. Due to the small grain size in volcanic rocks (apart from phenocrystals), chemical alteration of volcanic rocks mainly produces clay-size particles, which may be transported in suspension when the stream power is high enough, and deposited in low-energy fluvial environments [e.g., *Schumm et al.*, 2002]. However, not all outcrops of the Plateau Phyllosilicates are located in valleys. Besides, had the Plateau Phyllosilicates been deposited by water flowing in the valleys, they would have accumulated dominantly along valley floors, not along their walls. Additionally, the fact that Plateau Phyllosilicates crop out dominantly along valley walls, crater rims and other scarps

Figure 9. Spectral properties and morphology of the Al-phyllosilicate-rich member exposed on the Noachian plateau south of Coprates Chasma. (a) The Al-member is exposed at the surface of the Npl_2 unit, and below the Hr unit. The Al-member is probably located on the ejecta blanket of a large Noachian impact crater visible at the bottom right part of the image. Subsets of HRSC nadir images (orbits 100 and 982) overlain by CTX image P17_007574_1647. CRISM image FRT A51A is also displayed. Locations of Figures 9g and 9h are indicated. (b) False color image of the CRISM observation FRT A51A. (c) Close-up view of Figure 9b showing the Al-phyllosilicate-rich member. (d) Band depth map of the same observation (red, D2300; green, BD2200; blue, BD1900R). Stretched values: red, 0.001–0.009; green, 0.004–0.013; blue, 0.001–0.009. Cyan tones represent occurrences of Al-phyllosilicates, and blue tones represent occurrences of hydrated phases. (e) Close-up view of Figure 9d. (f) CRISM spectrum (average of 13 pixels divided by an average of 15 pixels of a neutral region) of Al-phyllosilicate compared to laboratory spectra (RELAB library spectra). Location of the averaged pixels is indicated by the arrow toward Figure 9e. (g) Subset of HiRISE Red image ESP_016800_1640 showing exposures of the light-toned Al-member on the plateau and along an impact crater rim (marked by an arrow; image center: −15.82°N, 54.44°W). (h) Contact between the Al-phyllosilicate-rich member and some material containing a hydrated phase. It is not clear whether the hydrated phase corresponds to the Al-member or to the Hr unit. Subset of HiRISE IRB color image PSP_0075741_1640 (image center: −15.8 °N, 54.35°W).
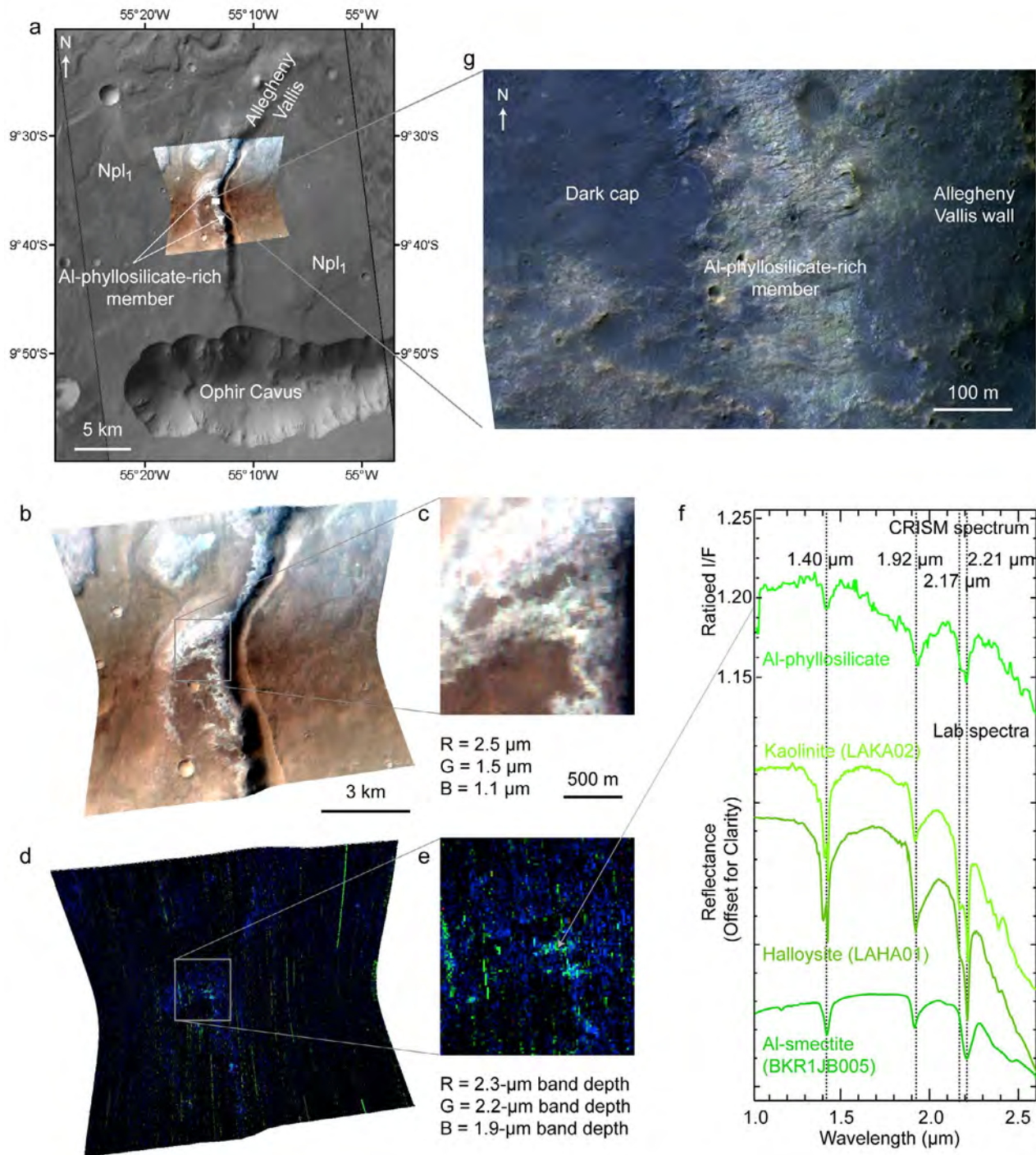
Figure 10. Spectral properties and morphology of the Al-phyllosilicate-rich member exposed along the wall of the outflow channel Allegheny Vallis. (a) Portion of the channel located north of Ophir Cavus. Subset of CTX image P20_009011_1703 overlain by CRISM image FRT B44D. Location of Figure 10g is indicated. (b) False color image of the CRISM observation FRT B44D showing outcrops of the Al-phyllosilicate-rich formation. (c) Close-up view of Figure 10b of the Al-phyllosilicate-rich member. (d) Band depth map of the same observation (red, D2300; green, BD2200; blue, BD1900R). Stretched values: red, 0.001–0.017; green, 0.001–0.02; blue, 0.003–0.022. Cyan tones represent occurrences of Al-phyllosilicates, and blue tones represent occurrences of hydrated phases. (e) Close-up view of Figure 10d of the Al-member in cyan. (f) CRISM spectrum (average of 64 pixels) of Al-phyllosilicate compared to laboratory spectra (RELAB library spectra). Location of the averaged pixels is indicated by the arrow toward Figure 10e. (g) Subset of HiRISE IRB color image PSP_009011_1705 showing the characteristic white, light blue to green tones of the Al-member exposed below a dark cap (image center: −9.6°N, 55.22°W).
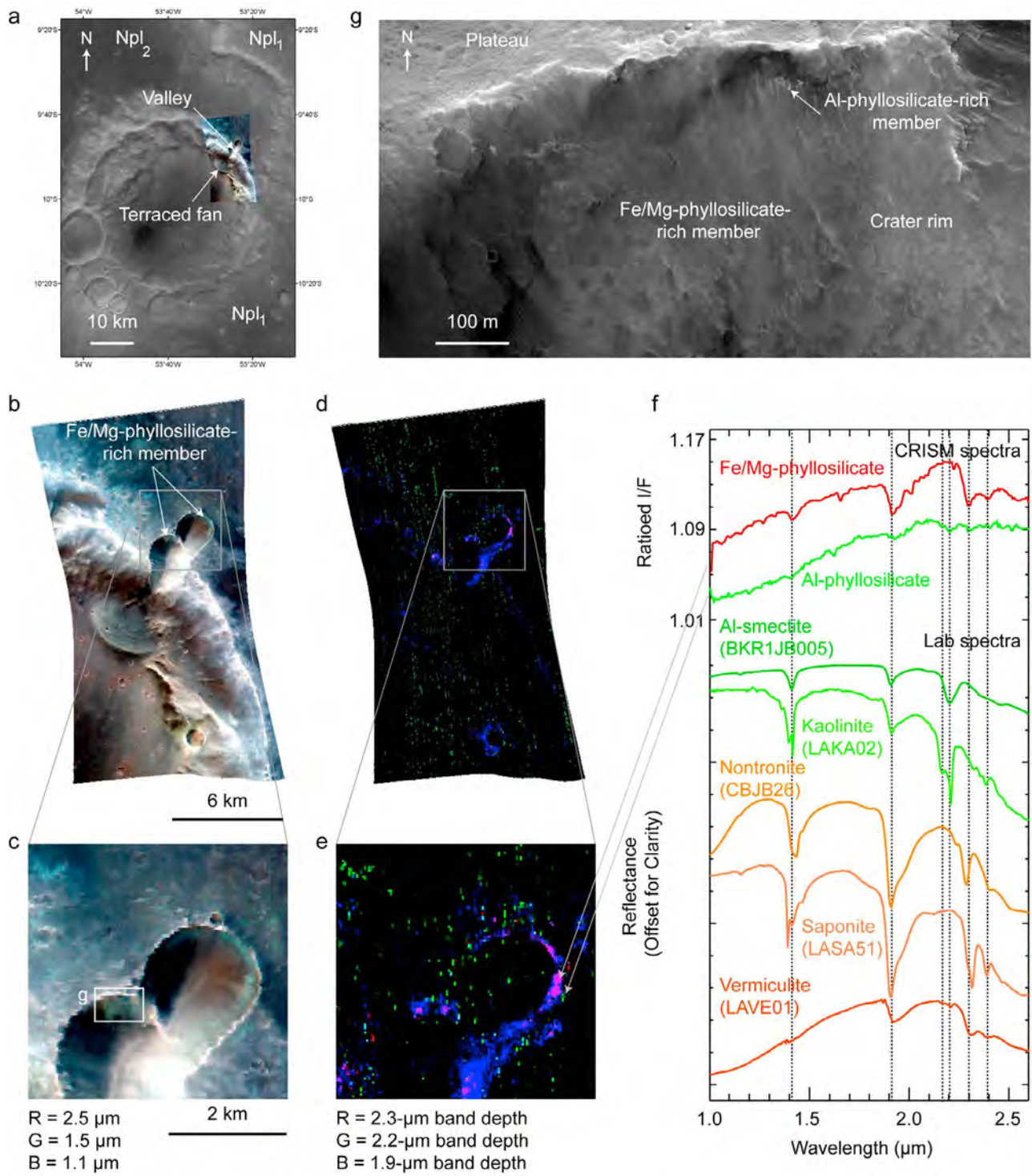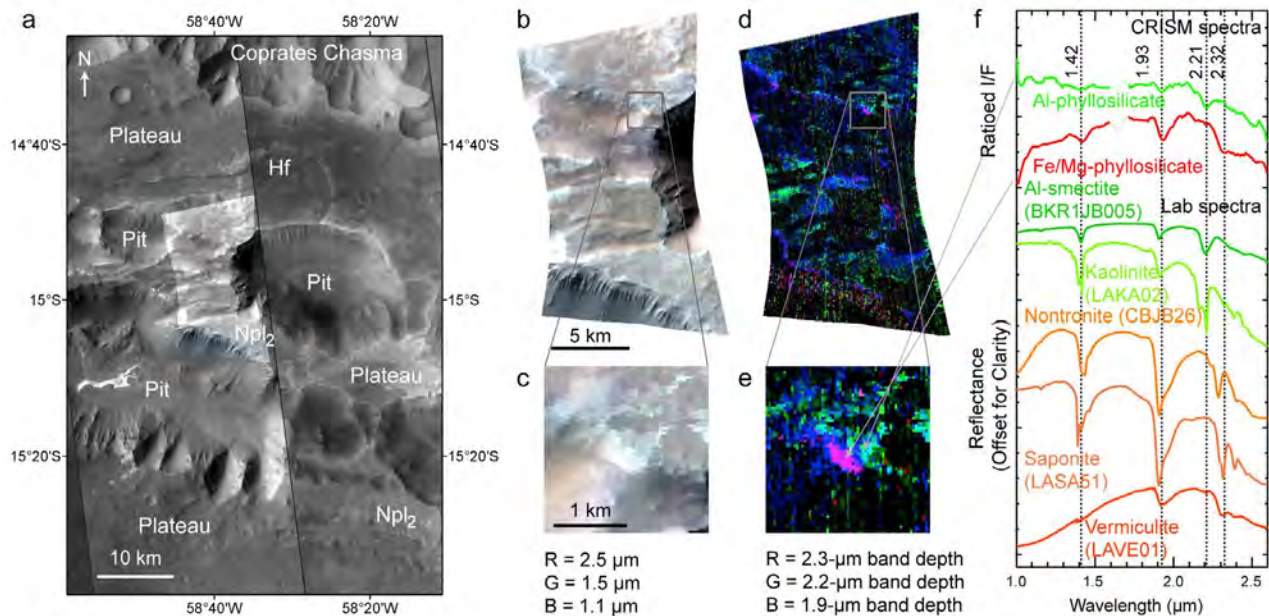
Figure 11

Figure 12. Spectral properties and morphology of the Al and Fe/Mg-phyllosilicate-rich members exposed on the upper part of the pit wall south of Coprates Chasma and on its surrounding plateau. (a) The Al-member is exposed on the Noachian unit Npl_2, which is locally overlain by the Hesperian unit Hf. Subset of CTX images P02_001957_1658 and P11_005214_1655 overlain by CRISM image HRL BECE. (b) False color image of the CRISM observation HRL BECE. (c) Close-up view of Figure 12b. (d) Band depth map of the same observation (red, D2300; green, BD2200; blue, BD1900R). Stretched values: red, 0.001–0.020; green, 0.001–0.034; blue, 0.002–0.019. Green and cyan tones represent occurrences of Al-phyllosilicates, purple tones of Fe/Mg-phyllosilicates, and blue tones of hydrated phases. (e) Close-up view of Figure 12d. (f) CRISM spectra of Al-phyllosilicates and of Fe/Mg-phyllosilicates compared to laboratory spectra (RELAB library spectra). Locations of the averaged pixels are indicated by arrows toward Figure 12e.

suggests that a phyllosilicate-rich layer formed regionally on top of the Noachian basement and was later exposed by carving of the valley systems and the formation of other scarps. Nevertheless, fluvial activity may have locally contributed to the genesis of phyllosilicates especially for those exposed on the gentle wall slopes of Allegheny Vallis that likely correspond to the river bed.

6.2. Hydrothermal Alteration

[33] Hydrothermal circulation may be related to magmatic processes of geodynamic origin or to impact cratering. Groundwater flow usually uses porosity fracture; in basaltic sequences this porosity results from cooling joints as well as contacts between successive lava flows or between the basal

flow and the underlying basement. Groundwater may also use intergranular porosity in tuff.

[34] Many secondary minerals may form by hydrothermal alteration, including most of those detected or suspected to be present in the study area based on CRISM spectra (montmorillonite, kaolinite, beidellite, nontronite, vermiculite). All of them, however, can form in other environments [e.g., *Anthony et al.*, 2003]. Sites of possible hydrothermal activity have been identified on Mars [*Marzo et al.*, 2010]. Although hydrothermal activity in these sites is thought to result from impact cratering, the alteration minerals formed if hydrothermal activity results from impact cratering are not significantly different from the minerals that would form by more classical, volcanic processes [*Naumov*, 2005]. Their

Figure 11. Spectral properties and morphology of the Al and Fe/Mg-phyllosilicate-rich members exposed along an impact crater rim, its connected valley wall and its surrounding plateau in Ophir Planum. (a) View of the impact crater located on Noachian terrains (Npl_1 and Npl_2 units). Subset of HRSC nadir image (orbit 100) overlain by CRISM image HRL 80CB. (b) False color image of the CRISM observation HRL 80CB. (c) Close-up view of Figure 11b. Location of Figure 11g is indicated. (d) Band depth map of the same observation (red, D2300; green, BD2200; blue, BD1900R). Stretched values: red, 0.001–0.013; green, 0.004–0.008; blue, 0.001–0.009. Green and cyan tones represent occurrences of Al-phyllosilicates, purple tones of Fe/Mg-phyllosilicates, and blue tones of hydrated phases. (e) Close-up view of Figure 11d. (f) CRISM spectra of Al-phyllosilicates (average of 2 pixels divided by an average of 4 pixels of a neutral region) and of Fe/Mg-phyllosilicates (average of 15 pixels divided by an average of 8 pixels of a neutral region) compared to laboratory spectra (RELAB library spectra). Locations of the averaged pixels are indicated by arrows toward Figure 11e. (g) Subset of HiRISE Red image PSP_005583_1700 showing the Fe/Mg-member exposed along the crater wall. The Al-member corresponds to a thin light layer exposed above the Fe/Mg-member (image center: −9.79°N, 53.41°W).
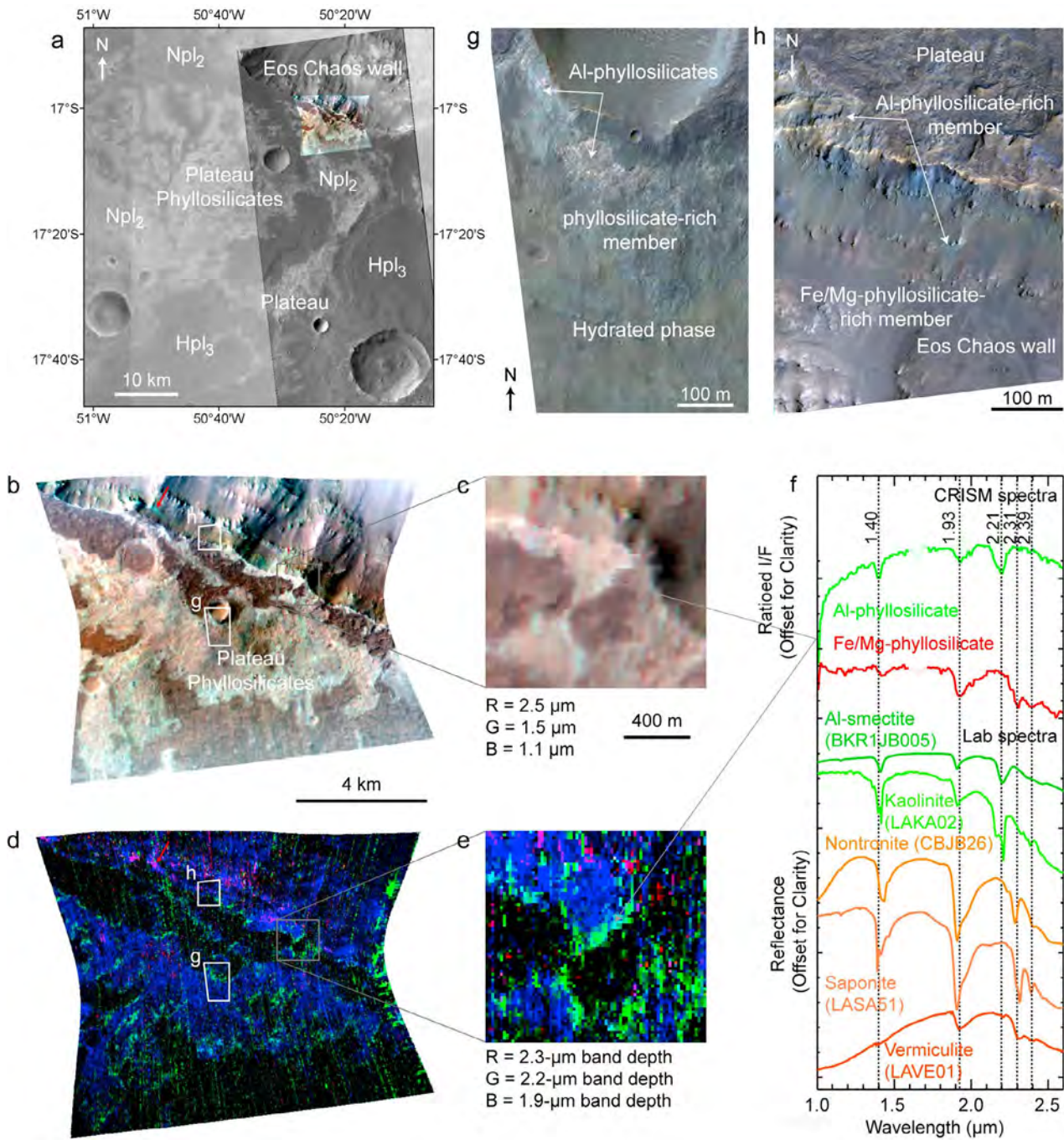
Figure 13

Table 2. Possible Formation Processes for the Plateau Phyllosilicates

Formation Process	Consistent Observations	Inconsistent/Limiting Observations
Surface water runoff	• Many outcrops located along valley systems	• Not all outcrops are located along valley systems • Phyllosilicates dominantly located along valley walls, not along valley floors
Hydrothermal alteration	• Often located on terrains surrounding large impact craters • Many secondary minerals that are expected are those detected (smectites, kaolinites, vermiculites). • Many outcrops are buried by lavas	• Extensive distribution • No prehnite, or chlorite detected • Phyllosilicates not always associated to impact craters and Hesperian lavas
Burial metamorphism Pedogenesis	• Extensive distribution • Extensive distribution • No initial structure of the parent rock such as layering preserved • Many secondary minerals that are expected are those detected (smectites, kaolinites, halloysites, vermiculites) • Observed mineralogical stratification	• No chlorite observed

bulk composition, however, obviously depends on the composition of the target rocks. The mineralogy of hydrothermal minerals formed as a consequence of impact cratering has been characterized at Toro crater [*Marzo et al.*, 2010]. It includes prehnite, chlorites, smectites, and opaline silica. No prehnite or chlorite have been detected in the study area, which means that if the basement rocks were similar in the study area and at Toro crater, the hydrothermal system would have reached temperatures lower than in Toro crater, but still capable of forming the observed smectites. No serpentine has been detected in our study area and *Schwenzer and Kring* [2009a, 2009b] showed by modeling that depending on the parent rock, serpentine is often expected to form by hydrothermalism on Mars. Whatever the mineral assemblage is, phyllosilicates may have not been formed by impact-induced hydrothermalism, in which case phyllosilicates would be typically observed in the central part of craters [e.g., *Naumov*, 2005; *Marzo et al.*, 2010], not on their rims nor outside the crater, where in contrast the Plateau Phyllosilicates are usually observed. These phyllosilicates are therefore more likely to have been merely exposed by impacts rather than formed by impact-related hydrothermalism.

[35] In many locations, Plateau Phyllosilicates are buried beneath thin units of dark Hesperian lavas (e.g., Figures 4, 7a, 7b, 7d, 8, and 13). Eruption of these Hesperian lavas may have caused deuteric alteration in the underlying Noachian substrate which led to formation and/or transformation of a thin layer of phyllosilicates at the interface between the Noachian basement and lava flows. This form of thermal metamorphism has been proposed to explain the formation of hydrated minerals in Nili Fossae at the interface with Syrtis Major flows [*Harvey and Griswold*, 2010]. This top-down cooking of Noachian material during the emplacement of Hesperian lava flows may have locally played a role in the formation of Plateau Phyllosilicates but only in a limited way. First, not all Plateau Phyllosilicates have been covered by Hesperian lavas. Second, only a limited thickness of material underlying the lava flow itself may have been altered by such a short-lived process occurring during the last stages of lava cooling. Another hypothesis is that Plateau Phyllosilicates correspond to volcanic ash deposited along the plateau that was subsequently altered by magmatic hydrothermal solutions to form phyllosilicates. This has been proposed for smectites located in Noctis Labyrinthus troughs [*Thollot et al.*, 2010; *Weitz et al.*, 2011]. However, the internal stratigraphy of Plateau Phyllosilicates constituted of a lower Fe/Mg-member and an upper Al-member is difficult to explain by hydrothermal/deuteric alteration alone.

6.3. Burial Metamorphism

[36] Sediments buried in subsiding basins undergo an increase of pressure and temperature that may eventually result in burial metamorphism [e.g., *Robinson and Bevins*, 1989; *Fielitz and Mansy*, 1999], by which smectite

Figure 13. Spectral properties and morphology of the Al and Fe/Mg-phyllosilicate-rich members exposed along the upper part of Eos Chasma wall and on its surrounding plateau. (a) The phyllosilicate-rich formation is exposed on the Noachian unit Npl2, which is locally overlain by the Hesperian unit Hpl$_3$. Subsets of HRSC nadir images (orbits 64 and 394) overlain by CTX image B02_010580_1625. CRISM image FRT D23E is also displayed. (b) False color image of the CRISM observation FRT D23E. Locations of Figures 13g and 13h are indicated. The red arrow indicates the location of the averaged pixels that have a corresponding spectrum characteristic of Fe/Mg-phyllosilicates displayed in Figure 13f. (c) Close-up view of Figure 13b. (d) Band depth map of the same observation (red, D2300; green, BD2200; blue, BD1900R). Stretched values: red, 0.001–0.019; green, 0.001–0.021; blue, 0.001–0.018. Green and cyan tones represent occurrences of Al-phyllosilicates, pink tones of Fe/Mg-phyllosilicates, and blue tones of hydrated phases. (e) Close-up view of Figure 13d. (f) CRISM spectra of Al-phyllosilicates (average of 12 pixels divided by an average of 12 pixels of a neutral region) and of Fe/Mg-phyllosilicates (average of 18 pixels divided by an average of 12 pixels of a neutral region) compared to laboratory spectra (RELAB library spectra). Locations of the averaged pixels are indicated by arrows toward Figure 13e for the Al-phyllosilicate spectra, and by a red arrow in Figures 13b and 13d for the Fe/Mg-phyllosilicate spectra. (g) Portion of HiRISE IRB color image PSP_010580_1630 showing a close-up view of the Al-member on the plateau (image center: −17.04°N, 50.37°W). (h) Portion of the same HiRISE image showing a close-up view of the Al-phyllosilicate-rich member on the plateau and along the upper part of Eos Chasma wall. The Fe/Mg-member appears topographically below the Al-member (image center: −17°N, 50.38°W).

transforms to illite. Chlorite may form as a by-product of the illitization reaction [*Weaver*, 1989].

[37] However, smectites are still present in the Plateau Phyllosilicates, while no illite or chlorite is observed. Illite spectra display vibrational absorptions bands at 1.4 μm, 2.2 μm and 2.35 μm, which are not present in CRISM spectra. Even if the absence of illite (K-rich) in Plateau Phyllosilicates may be related to the depletion in K of the upper crust compared to Earth's [e.g., *Hahn et al.*, 2007], the lack of chlorite implies that burial metamorphism is not a relevant formation process for the Plateau Phyllosilicates.

6.4. Pedogenesis

[38] On Earth, a very common process to form phyllosilicates is by weathering of rocks due to percolating waters. Volcanic materials and impact breccia correspond to very permeable bedrock, which is very sensitive to weathering. On Earth, soils of volcanic origin (andosols) are grayish and of various thicknesses [*Quantin*, 1972; *Chamley*, 1989]. Meteoric waters or melted snow infiltrate the bedrock and weather it, with soluble ions such as Na^+, K^+, and Mg^{2+} migrating from the top to the bottom of the alteration series. Fe/Mg-smectites form in accumulation horizons corresponding to confined environments. Hence, they are generally preserved in the poorly drained, lowest part of andosols [e.g., *Carroll*, 1970; *Quantin et al.*, 1975]. They generally form in neutral to alkaline environments [e.g., *Weaver*, 1989]. Al^{3+} is less mobile and remains generally in the upper part of andosols, where Al-smectites such as montmorillonites and beidellites form. The last steps of andosol development consist in the formation of halloysite, a hydrated form of kaolinite, followed by the formation of kaolinite and gibbsite. Kaolinite typically forms in areas of active leaching, where the drainage is intense at the top of the altered series under slightly acidic conditions [*Swayze et al.*, 2002; *McKeown et al.*, 2009; *Altheide et al.*, 2010]. Gibbsite is generally observed in very mature soils. It has not been detected in the study area.

[39] This internal stratification of weathering products is also classically observed in terrestrial tropical soils, where percolation of surface water produces leaching of the superficial soil horizons, and relative concentration of Al in yellow laterite. Concomitantly, Fe^{3+} may accumulate above the yellow laterite as hematite, and form a duricrust overlying a pisolite-rich level (red laterite). Applied to Mars, a model of lateritic soil forming at the top of the Noachian crust applied to the Plateau Phyllosilicates would imply that Al accumulates at the surface in the form of montmorillonite and other variously hydrated Al-rich phyllosilicates such as beidellite, kaolinite, and halloysite. In this model, Iron would migrate downward during periods of high water table, and would accumulate later during periods of low water table as Fe and Mg-rich phyllosilicates, such as nontronite and vermiculite. However, hematite and goethite are frequently associated to terrestrial laterites; these have not been detected in the study area. No duricrust has been observed either. These observations suggest that, if a lateritic model is correct for the Plateau phyllosilicates, these have probably been formed under different morphogenetic conditions (e.g., climate, water circulations) than terrestrial laterites.

[40] The formation of phyllosilicates by pedogenesis is consistent with many of our observations about the Plateau Phyllosilicates. These are widespread at the surface. This is consistent with a water source available on extended areas such as precipitations contrary to hydrothermal fluids, which would be more localized. This is also consistent with the fact that Plateau Phyllosilicates were never buried under a very thick sequence of rocks, as is demonstrated by the fact that they lack metamorphic minerals. Upon desiccation, vermiculite compaction may form the observed polygons (Figures 3b,3e, 6g, and 11g); similarly, montmorillonite forming in the soil may desiccate and form the polygons observed on Figures 7a–7c, 9g, and 10g. The massive aspect of the Plateau Phyllosilicates in a number of sites (e.g., Figures 3, 11, 13) is consistent with extensive pedogenesis, which is known for destroying the initial structure such as layering of the parent rock [*Righi and Meunier*, 1995]. At last, the main observation that is consistent with formation by pedogenesis is the mineralogical stratigraphy of smectites, vermiculites, and kaolinites, which is characteristic of the alteration sequence of basaltic andosols on Earth.

[41] The Plateau Phyllosilicates attest to the widespread surface alteration of the Noachian basement, probably by pedogenesis, in the region of Valles Marineris. This kind of Plateau Phyllosilicates has also been described in other regions of Mars including Mawrth Vallis [*Loizeau et al.*, 2007; *McKeown et al.*, 2009; *Noe Dobrea et al.*, 2010], Nili Fossae [*Ehlmann et al.*, 2009; *Gaudin et al.*, 2011], western Arabia Terra [*Noe Dobrea et al.*, 2010], and northeast Noachis Terra [*Wray et al.*, 2009]. This widespread distribution of Plateau Phyllosilicates gives evidence that pedogenic alteration of the Noachian basement occurred on a regional scale at some time in the Martian history.

7. Stratigraphical Relationships With Other Sedimentary Formations

7.1. The Light-Toned Unit

[42] From the regional map of *Scott and Tanaka* [1986] and the analysis of CTX and HiRISE images, the dark cap covering the Plateau Phyllosilicates corresponds to Hesperian volcanic lavas. It is locally overlain by thin and small exposures of a light-toned material, which is polygonally fractured (Figure 14). This light-toned unit is observed on several locations in Ophir Planum and Margaritifer Terra and may correspond to late deposition of material over the plateaus during the Hesperian Epoch. This thin light-toned material is spectrally neutral (Figure 14e–14h) and morphologically similar to proposed chloride-bearing material observed by the THEMIS instrument that also occur stratigraphically above phyllosilicate-rich formations [*Osterloo et al.*, 2008, 2010; *Glotch et al.*, 2010] (Figure 14c). As suggested for the proposed chloride-bearing material by *Osterloo et al.* [2010], the thin light-toned material may result from surface runoff and/or groundwater upwelling, then water accumulation in ponds, brine concentration by water evaporation, and precipitation.

7.2. The Layered Deposits (LDs)

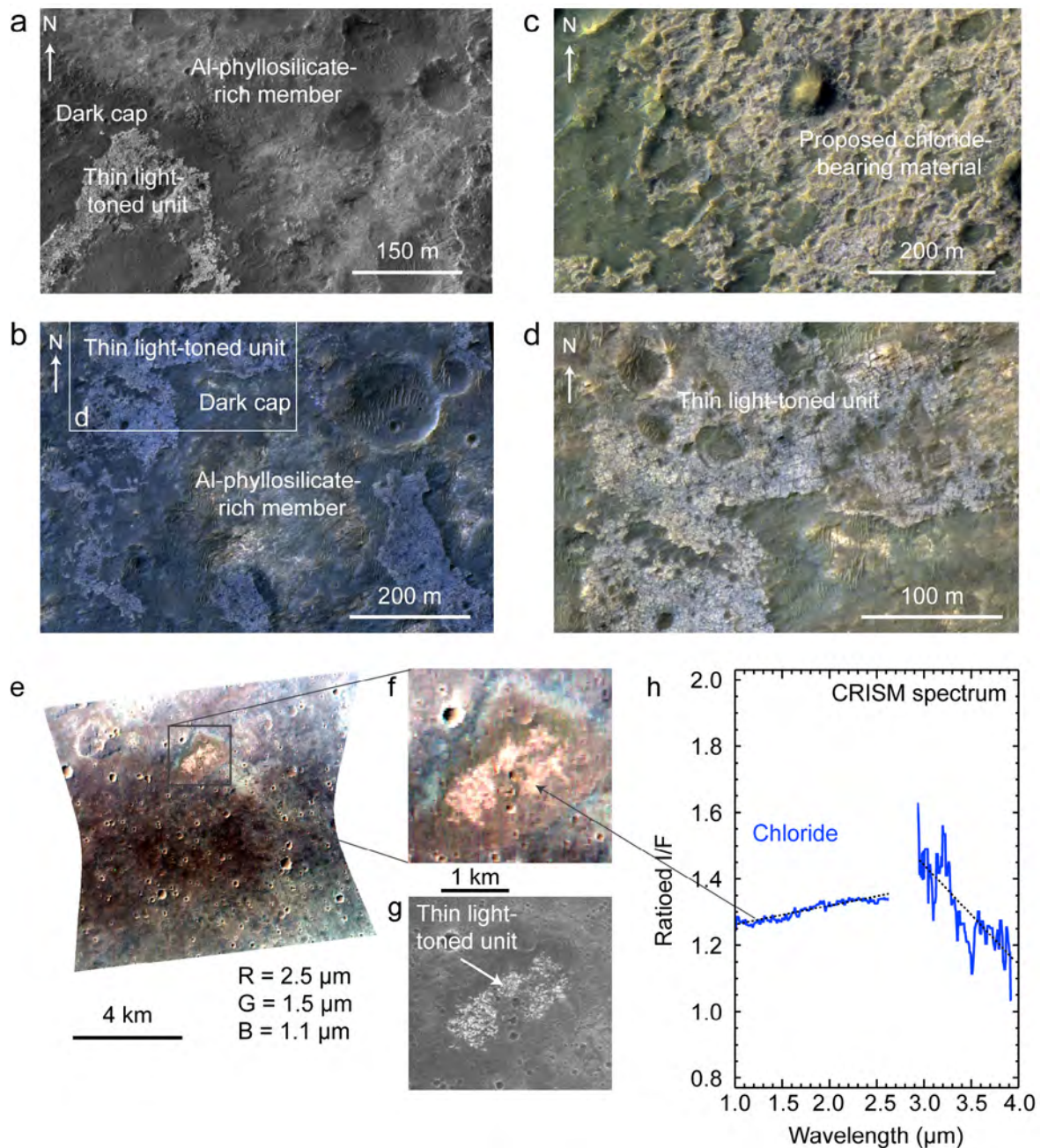[43] Located on Noachian-aged terrains, the Plateau Phyllosilicates are stratigraphically below the Layered Deposits

Figure 14. Thin light-toned unit stratigraphically above the Al-member that has morphological similarities with chloride-rich material. (a) Portion of HIRISE Red image PSP_010079_1725 (image center: −7.63°N, 54.04°W). (b) Thin light-toned unit, polygonally fractured, and light blue on this portion of HIRISE IRB color image ESP_016593_1700 (image center: −10.1°N, 52.3°W). (c) Portion of HIRISE IRB color image PSP_005680_1525 showing proposed chloride-bearing material in Terra Cimmeria described in *Osterloo et al.* [2010] (image center: −27.2°N, 179.5°W). (d) Close-up view of Figure 14b showing in more details the thin light-toned unit. (e) False color image of the CRISM observation FRT B23E showing an outcrop of thin light-toned unit located in Margaritifer Terra that possibly contains chlorides (image center: −20.15°N, 49.61°W). This detection is reported in *Osterloo et al.* [2010, Figure 9]. (f) Close-up view of the chloride-rich thin light-toned unit shown in Figure 14e. (g) Portion of CTX image P11_005517_1620 showing a close-up view of the proposed chloride-bearing thin light-toned unit (image center: −20.11°N, 49.62°W). (h) CRISM spectrum of the thin light-toned unit (average of 25 pixels divided by an average of 8 pixels of a neutral region). This spectrum is featureless, sloped and does not display any strong 3 μm hydration feature, which is consistent with an anhydrous phase such as chlorides [*Murchie et al.*, 2009a; *Glotch et al.*, 2010; *Osterloo et al.*, 2010]. Locations of the averaged pixels are indicated by arrows toward Figure 14f.
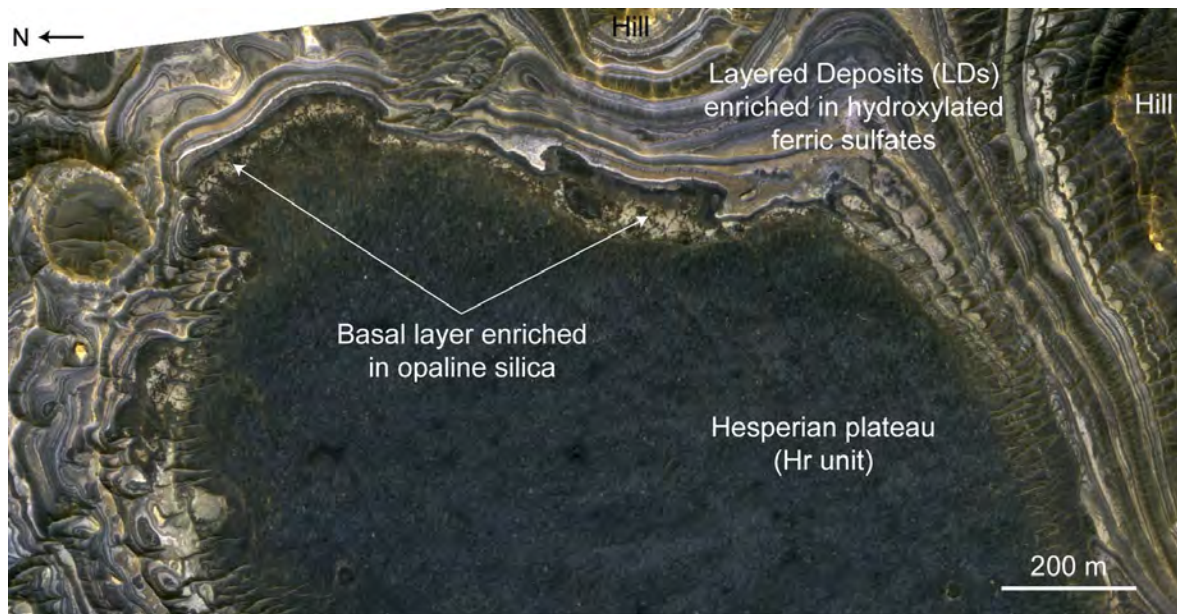
Figure 15. Layered Deposits (LDs) containing hydroxylated ferric sulfates [*Milliken et al.*, 2008; *Bishop et al.*, 2009] located west of Juventae Chasma stratigraphically above the Hesperian basement (Hr unit). The basal unit of the LDs contains opaline silica [*Bishop et al.*, 2009]. Portion of HiRISE IRB color image PSP_003434_1755 (image center: −4.7°N, 63.6°W).

(LDs) (Figure 2). The LDs consist of a 100 m thick series of alternating light and dark beds that cover the plateaus surrounding Valles Marineris north of Tithonium Chasma, south of Ius Chasma, around West Candor Chasma, and southwest of Juventae Chasma and Ganges Chasma (Figure 15) [*Milliken et al.*, 2008; *Bishop et al.*, 2009; *Weitz et al.*, 2008, 2010, *Le Deit et al.*, 2010c]. Their stratigraphic relationships with the plateaus and the Valles Marineris chasmata indicate that the LDs were deposited during the Early to Late Hesperian, and possibly later depending on the region. Near Juventae Chasma they were deposited before the end of the backwasting of the walls, and near Ius Chasma they were probably deposited before the formation of Louros Valles by sapping. Because of their huge spatial coverage (~42,300 km² at least) and their high elevated plateau setting, *Le Deit et al.* [2010c] suggested that LDs correspond to air fall dust and/or volcanic ash. The association of all LDs with valley systems and the occurrence of LDs within inverted channels indicate that at least portions of LDs are fluvial in origin [e.g., *Weitz et al.*, 2008, 2010]. In addition to valley systems and inverted channels, the surface of the LDs is characterized by various morphological features, including lobate ejecta and pedestal craters, polygonal fractures, which are all consistent with liquid water and/or water ice filling the pores of LDs. The LDs were episodically eroded by fluvial processes and were possibly modified by sublimation processes [*Le Deit et al.*, 2010c]. The analysis of CRISM data showed that the LDs contain amorphous silica such as opal, and hydroxylated ferric sulfates in various proportions depending on the region. West of Juventae Chasma, the basal layer of LDs contains opaline silica and the layers above contain hydroxylated ferric sulfates (Figure 15) [*Bishop et al.*, 2009]. These mineral phases are consistent with aqueous alteration by sulphur-rich acidic solutions under

oxidizing conditions of unaltered basaltic substrate [e.g., *Tosca et al.*, 2004] or phyllosilicate-rich substrate. Experimental studies by *Altheide et al.* [2010] showed indeed that nontronite is fully degraded under acid leaching at pH ≤ 4, resulting in a mixture of hydrated amorphous silica and Al- and Fe-sulfates.

8. Implications for Climate and Timing of Events

8.1. A Temperate-Subarid Climate During the Noachian Epoch

[44] The mineral assemblages that we observe on the plateaus around Valles Marineris can provide clues to the Martian climate since the formation of these minerals until present. In addition to the initial mineralogical composition of the parent rock, age, and topography, the climate (temperature, humidity, and seasons) also influences the degree of weathering and alteration, and the type of soil formed by alteration [e.g., *Chamley*, 1989; *Velde*, 1992]. In temperate-humid and warm-subarid climates (usually in mid- to low-latitude regions on Earth), surface rocks are submitted to alternation of wet and dry seasons implying discontinuous weathering processes. In the resulting soils (vertisols), the pH tends to increase downward, from slightly acid to alkaline values. The clay mineralogy is characterized by the neo-formation of well-crystallized smectites regardless of the nature of the parent rocks [e.g., *Paquet*, 1970; *Chamley*, 1989], as well as vermiculites and irregular mixed-layers [*Chamley*, 1989]. As a result, Fe/Mg- and Al-smectites form abundantly on volcanic rocks under temperate-warm to cool climates. But iron smectites (e.g., nontronite) are only preserved in environments that are not too hot or too humid in andosols [*Chamley*, 1989]. For instance, *Quantin et al.* [1975] observed iron smectites in the New Hebrides only
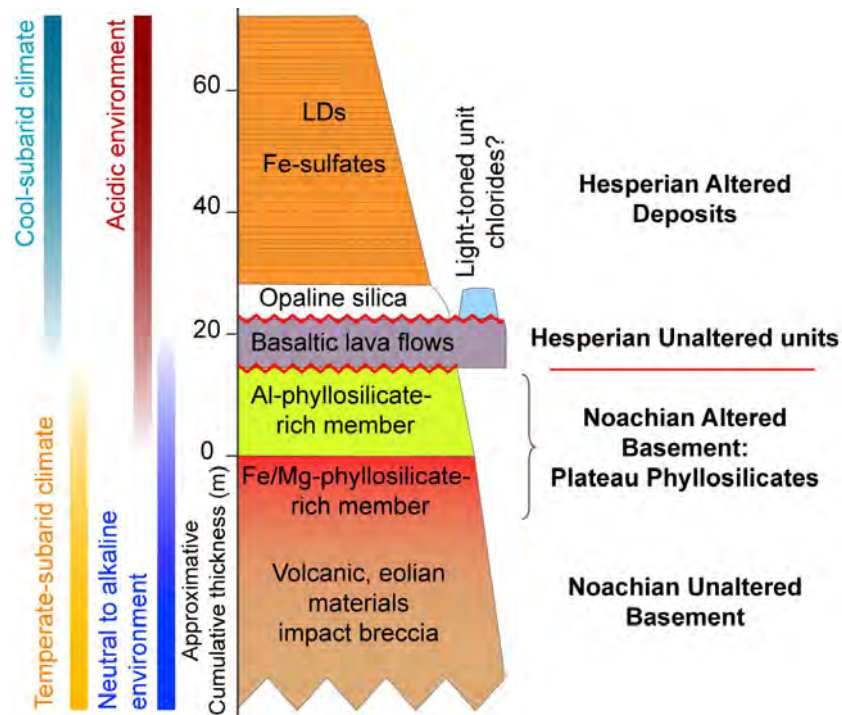
Figure 16. Stratigraphic log of the upper part of the plateaus surrounding Valles Marineris.

within andosols poorly drained and submitted to subarid conditions. Hence, the presence of nontronite in the Fe/Mg-member of the Plateau Phyllosilicates suggests that this member formed under a subarid climate, or even a possibly dryer climate (Figure 16). This also suggests that the Fe/Mg-member was not exposed to a humid climate since it was exposed at the surface. The Al-member locally contains kaolinite. Under temperate climates, pedogenic kaolinite is never very abundant, but develops more extensively and rapidly at the expense of volcanic rocks than of others [*Hétier et al.*, 1977; *Chamley*, 1989]. Consequently, it is reasonable to conclude that the Plateau Phyllosilicates mainly formed under a temperate and subarid climate during the Noachian Epoch.

8.2. A Cool-Subarid Climate During the Hesperian Epoch

[45] Many outcrops containing phyllosilicates are located close to material containing a hydrated phase but far from the protective cap and for which we couldn't determine the exact nature (e.g., Figures 2, 5, 7, 8, and 13). This hydrated phase may correspond to a residual phase of the phyllosilicates produced by alteration of the Plateau Phyllosilicates after their exhumations. In other words, the weathering of the Plateau Phyllosilicates probably continued on their exhumed outcrops during the Hesperian Epoch. The light-toned units (possibly chloride-rich evaporites) and the LDs (Fe-sulfate and opaline silica-rich) also attest to aqueous activity on the plateaus during the Hesperian Epoch (Figure 16). The presence of these evaporites requires a climate with an alternation of wetting and drying stages, which is consistent with a subarid climate [e.g., *Sonnenfeld*, 1984; *Gutiérrez*, 2005]. Under a cool climate on Earth, many secondary silica such as opal or cristobalite precipitate under acid and oxidant

conditions in podzols whatever the initial composition of the parent rock [e.g., *Swindale and Jackson*, 1960]. Hence, the occurrence of Fe-sulfates and opaline silica in the LDs is consistent with an alteration under acidic, oxidizing and low temperature conditions [e.g., *Milliken et al.*, 2008]. Since this alteration occurred on the plateaus at the Hesperian Epoch, we can wonder why the extended units of Hesperian volcanic units (e.g., Hr, Hpl$_3$) forming the dark cap over the Plateau Phyllosilicates do not keep any record of this alteration. This can be explained by the fact that the exposed Noachian units (volcanic and eolian materials and impact breccia that are rich in impact glasses), as well as the fine-grained material constituting the LDs (volcanic ash and/or dust) are much less resistant to weathering than volcanic lavas.

8.3. Timing of Events

[46] We propose the following timing of events (Figure 17):

[47] (1) During the Noachian Epoch, episodes of aqueous activity under a temperate-subarid climate induce the weathering of the Noachian units. Fe/Mg- and Al-phyllosilicates of the Plateau Phyllosilicates formation are produced by pedogenesis under neutral to alkaline environment. Kaolinite and/or halloysite form in areas of more intense drainage at the surface under slightly acidic environments.

[48] (2) During the Hesperian Epoch, extensive lava flows partially bury the Plateau Phyllosilicates. Phyllosilicates may locally form by deuteric alteration. The climate is still subarid and cooling.

[49] (3) Valles Marineris and surrounding pits form and expose the Plateau Phyllosilicates along their walls. Extensive volcanic ash and dust deposits cover the Hesperian lava flows. Sulphur-rich acidic solutions alter the LDs and form opaline silica and Fe-sulfates. The Hesperian lavas are eroded
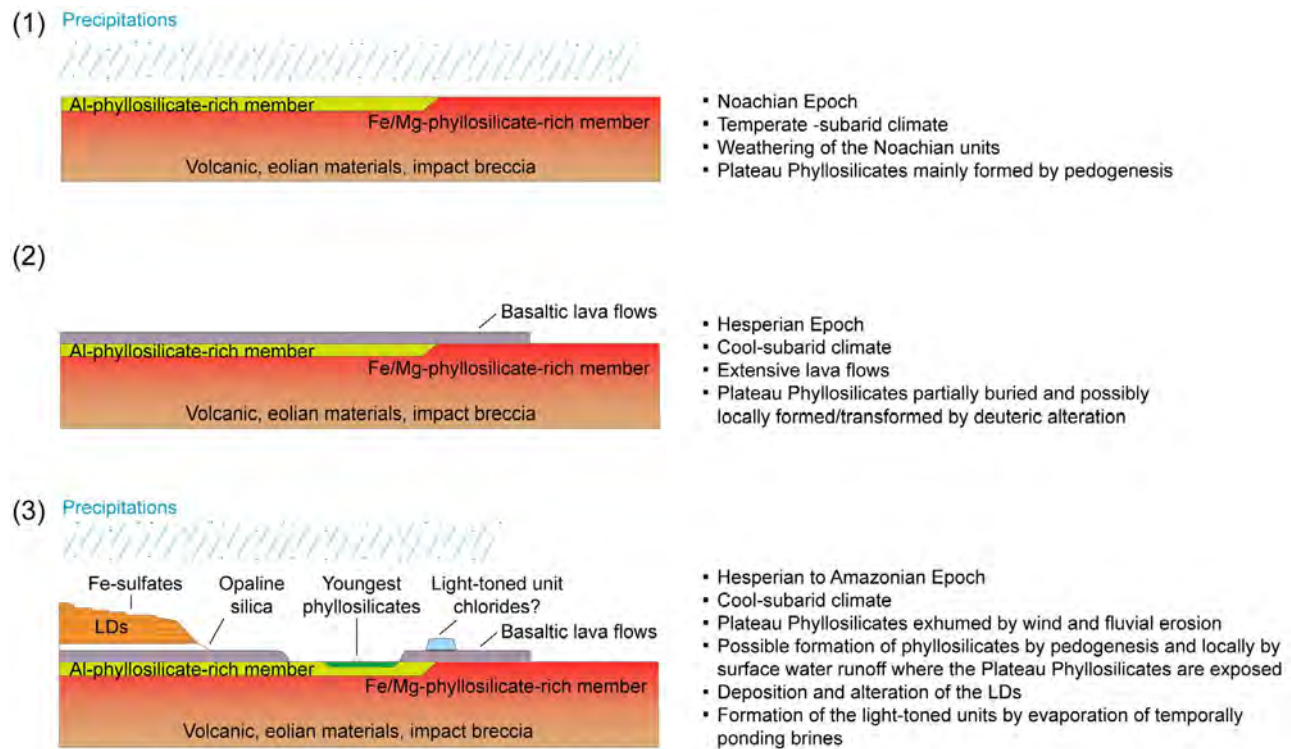
Figure 17. Sketches illustrating the proposed timing of events on the plateaus surrounding Valles Marineris. Not to scale.

and the Plateau Phyllosilicates that were buried are exhumed. Impact and fluvial events also exhume Plateau Phyllosilicates along crater and valley walls. Kaolinite and/or halloysite may form where the Plateau Phyllosilicates are exposed, possibly in fluvial environments locally. The light-toned units form by evaporation of temporally ponding brines.

[50] (4) The climate continues to cool down and the precipitations become scarcer until the present-day conditions are reached. Erosion of the plateaus continues.

9. Conclusion

[51] The geological study of the plateaus around Valles Marineris reveals the occurrence of an extensive light-toned phyllosilicate-rich formation, the Plateau Phyllosilicates, covering $\sim$197,000 km^2 at minimum. Tens of meters in thickness, this formation is located at various elevations (between $-$2798 m and 3363 m). It lies on top of the Noachian basement (mainly units Npl_1 and Npl_2 corresponding to volcanic and eolian materials, and impact breccia), either as flat exposures on plateaus (Ophir Planum, Thaumasia Planum, Margaritifer Terra), or along slopes such as valley walls (Allegheny Vallis, Shalbatana Vallis, Her Desher Vallis, Nirgal Vallis), chasma walls (Ganges Chasma, Coprates Chasma, Eos Chaos), pit walls and impact crater rims. The Plateau Phyllosilicates comprise two members. The upper member contains Al-phyllosilicates (Al-smectites - montmorillonite, beidellite-, kaolinite and/or halloysite) and the lower member contains Fe/Mg-phyllosilicates (Fe/Mg-smectites - nontronite, saponite- and vermiculite). From these

observations and by analogy with terrestrial processes, we suggest that the Plateau Phyllosilicates formed by pedogenesis related to the weathering of the Noachian bedrock by percolation of episodic meteoric water or melted snow through time. During the Noachian Epoch, the Plateau Phyllosilicates developed in a neutral to alkaline environment under a temperate and subarid climate. Kaolinite formed in areas of more intense drainage at the surface under a slightly acidic environment. During the Hesperian Epoch, the water availability was still limited and the alteration of the plateaus continued under a cooling environment. Eruption of lavas may have caused deuteric alteration in the underlying Noachian substrate at a local scale and form phyllosilicates. Kaolinite and/or halloysite may have formed by acid alteration of the exhumed Plateau Phyllosilicates, possibly in fluvial environments locally. A light-toned unit formed by evaporation of temporally ponding brines. Layered deposits mainly corresponding to volcanic ash and or dust were altered by sulphur-rich acidic solutions and formed Fe-sulfates and opaline silica.

References

Altheide, T. S., V. F. Chevrier, and E. Noe Dobrea (2010), Mineralogical characterization of acid weathered phyllosilicates with implications for secondary Martian deposits, *Geochim. Cosmochim. Acta*, 74, 6232–6248, doi:10.1016/j.gca.2010.08.005.

Anthony, J. W., R. A. Bideaux, K. W. Bladh, and M. C. Nichols (2003), *Handbook of Mineralogy*, vol. II, 904 pp., Mineral. Soc. of Am., Washington, D. C.

Barnhart, C. J., and F. Nimmo (2011), Role of impact excavation in distributing clays over Noachian surfaces, *J. Geophys. Res.*, 116, E01009, doi:10.1029/2010JE003629.

Bibring, J.-P., Y. Langevin, J. F. Mustard, F. Poulet, R. Arvidson, A. Gendrin, B. Gondet, N. Mangold, P. Pinet, and F. Forget (2006), Global mineralogical and aqueous Mars history derived from OMEGA/Mars Express data, *Science*, 312, 400–404, doi:10.1126/science.1122659.

Bishop, J. L., C. M. Pieters, and R. G. Burns (1993), Reflectance and Mössbauer spectroscopy of ferrihydrite-montmorillonite assemblages as Mars soil analog materials, *Geochim. Cosmochim. Acta*, 57, 4583–4595, doi:10.1016/0016-7037(93)90184-X.

Bishop, J. L., et al. (2008a), Phyllosilicate diversity and past aqueous activity revealed at Mawrth Vallis, Mars, *Science*, 321, 830–833, doi:10.1126/science.1159699.

Bishop, J. L., M. D. Lane, M. D. Dyar, and A. J. Brown (2008b), Reflectance and emission spectroscopy of four groups of phyllosilicates: Smectites, kaolinite-serpentines, chlorites and micas, *Clay Miner.*, 43, 35–54, doi:10.1180/claymin.2008.043.1.03.

Bishop, J. L., et al. (2009), Mineralogy of Juventae Chasma: Sulfates in the light-toned mounds, mafic minerals in the bedrock, and hydrated silica and hydroxylated ferric sulfate on the plateau, *J. Geophys. Res.*, 114, E00D09, doi:10.1029/2009JE003352.

Bishop, J. L., W. P. Gates, H. D. Makarewicz, N. K. McKeown, and T. Hiroi (2011), Reflectance spectroscopy of beidellites and their importance for Mars, *Clays Clay Miner.*, 59, 378–399, doi:10.1346/CCMN.2011.0590403.

Buczkowski, D., and K. Seelos (2010), Extensive phyllosilicate layer in north-western Noachis Terra: Relationship to phyllosilicates in Holden and Eberswalde?, presented at the 4th MSL Landing site workshop, NASA, Monrovia, Calif., 27–29 September.

Buczkowski, D., K. D. Seelos, S. L. Murchie, F. P. Seelos, E. Malaret, C. Hash, and the CRISM team (2010), Extensive Phyllosilicate-bearing Layer Exposed by Valley Systems in Northwest Noachis Terra, *Lunar Planet. Sci.*, XLI, Abstract 1458.

Carroll, D. (1970), Clay minerals in Arctic Ocean sea-floor sediments, *J. Sediment. Petrol.*, 40, 814–821.

Carter, J., F. Poulet, J.-P. Bibring, S. Murchie, Y. Langevin, J. F. Mustard, and B. Gondet (2009), Phyllosilicates and other hydrated minerals on Mars: 1. Global distribution as seen by MEx/OMEGA, *Lunar Planet. Sci.*, XL, Abstract 2028.

Chamley, H. (1989), *Clay Sedimentology*, 623 pp., Springer, New York.

Clark, R. N., T. V. V. King, M. Klejwa, G. A. Swayze, and N. Vergo (1990), High spectral resolution reflectance spectroscopy of minerals, *J. Geophys. Res.*, 95, 12,653–12,680, doi:10.1029/JB095iB08p12653.

Dohm, J. M., K. L. Tanaka, and T. M. Hare (2001), Geologic map of the Thaumasia region of Mars, *U.S. Geol. Surv. Misc. Geol. Invest. Map*, I-2650, scale 1:5,000,000.

Ehlmann, B. L., et al. (2009), Identification of hydrated silicate minerals on Mars using MRO-CRISM: Geologic context near Nili Fossae and implications for aqueous alteration, *J. Geophys. Res.*, 114, E00D08, doi:10.1029/2009JE003339.

Fielitz, W., and J.-L. Mansy (1999), Pre- and synorogenic burial metamorphism in the Ardenne and neighbouring areas (Rhenohercynian zone, central European Variscides), *Tectonophysics*, 309, 227–256, doi:10.1016/S0040-1951(99)00141-9.

Flahaut, J., C. Quantin, H. Clenet, P. Allemand, J. F. Mustard, and P. Thomas (2012), Pristine Noachian crust and key geologic transitions in the lower walls of Valles Marineris: Insights into early igneous processes on Mars, *Icarus*, doi:10.1016/j.icarus.2011.12.027, in press.

Gaudin, A., E. Dehouck, and N. Mangold (2011), Evidence for weathering on Early Mars from a comparison with terrestrial weathering profiles, *Icarus*, 216, 257–268, doi:10.1016/j.icarus.2011.09.004.

Giese, R. F. (1988), Kaolin minerals: Structures and stabilities, in *Reviews in Mineralogy*, vol. 19, *Hydrous Phyllosilicates (Exclusive of Micas)*, edited by S. W. Bailey, pp. 29–62, Mineral. Soc. of Am., Washington, D. C.

Glotch, T. D., J. L. Bandfield, L. L. Tornabene, H. B. Jensen, and F. P. Seelos (2010), Distribution and formation of chlorides and phyllosilicates in Terra Sirenum, Mars, *Geophys. Res. Lett.*, 37, L16202, doi:10.1029/2010GL044557.

Grant, J. A., D. Buczkowski, R. P. Irwin III, and K. Siebach (2010), A lake in Uzboi Vallis and implications for late Noachian climate on Mars, *Lunar Planet. Sci.*, XLI, Abstract 1834.

Gutiérrez, M. (2005), *Climatic Geomorphology, Developments in Earth Science Processes*, 760 pp., Elsevier, New York.

Hahn, B. C., et al. (2007), Mars Odyssey Gamma Ray Spectrometer elemental relative surface age: Implications for Martian crustal evolution, *J. Geophys. Res.*, 112, E03S11, doi:10.1029/2006JE002821.

Harvey, R. P., and J. Griswold (2010), Burial, exhumation, metamorphism and other dastardly deeds exposed at the Hesperian/Noachian boundary in the southern Nili Fossae region, *Lunar Planet. Sci.*, XLI, Abstract 2045.

Hétier, J. M., N. Yoshinaga, and F. Weber (1977), Formation of clay minerals in andosoils under temperate climates, *Clay Miner.*, 12, 299–307, doi:10.1180/claymin.1977.012.4.03.

Le Deit, L., J. Flahaut, C. Quantin, and P. Allemand (2010a), Geological setting of different phyllosilicate-rich deposits exposed on the surrounding plateaus and in the walls of Valles Marineris, Mars, *Lunar Planet. Sci.*, XLI, Abstract 1146.

Le Deit, L., J. Flahaut, C. Quantin, O. Bourgeois, and E. Hauber (2010b), Geologic analysis of various hydrated formations exposed on the plateaus surrounding Valles Marineris, Mars, Abstract 6032, presented at the First International Conference on Mars Sedimentology and Stratigraphy, Lunar and Planet. Inst., El Paso, Tex., 19–21 April.

Le Deit, L., O. Bourgeois, D. Mège, E. Hauber, S. Le Mouélic, M. Massé, R. Jaumann, and J.-P. Bibring (2010c), Geological history of a layered formation covering the plateaus around Valles Marineris, Mars, *Icarus*, 208, 684–703, doi:10.1016/j.icarus.2010.03.012.

Loizeau, D., et al. (2007), Phyllosilicates in the Mawrth Vallis region of Mars, *J. Geophys. Res.*, 112, E08S08, doi:10.1029/2006JE002877.

Loizeau, D., N. Mangold, F. Poulet, V. Ansan, E. Hauber, J.-P. Bibring, B. Gondet, Y. Langevin, P. Masson, and G. Neukum (2010), Stratigraphy in the Mawrth Vallis region through OMEGA, HRSC color imagery and DTM, *Icarus*, 205, 396–418, doi:10.1016/j.icarus.2009.04.018.

Loizeau, D., J. Carter, S. Bouley, N. Mangold, F. Poulet, J.-P. Bibring, F. Costard, Y. Langevin, B. Gondet, and S. L. Murchie (2012), Characterization of hydrated silicates-bearing outcrops in Tyrrhena Terra, Mars: Implication to the alteration history of Mars, *Icarus*, in press.

Malin, M. C., et al. (2007), Context camera investigation on board the Mars Reconnaissance Orbiter, *J. Geophys. Res.*, 112, E05S04. doi:10.1029/2006JE002808.

Marzo, G. A., A. F. Davila, L. L. Tornabende, J. M. Dohm, A. G. Fairén, C. Gross, T. Kneissl, J. L. Bishop, T. L. Roush, and C. P. McKay (2010), Evidence for Hesperian impact-induced hydrothermalism on Mars, *Icarus*, 208, 667–683, doi:10.1016/j.icarus.2010.03.013.

McEwen, A. S., et al. (2007), Mars Reconnaissance Orbiter's High Resolution Imaging Science Experiment (HiRISE), *J. Geophys. Res.*, 112, E05S02, doi:10.1029/2005JE002605.

McGuire, P. C., et al. (2009), An improvement to the volcano-scan algorithm for atmospheric correction of CRISM and OMEGA spectral data, *Planet. Space Sci.*, 57, 809–815, doi:10.1016/j.pss.2009.03.007.

McKeown, N. K., J. L. Bishop, E. Z. Noe Dobrea, B. L. Ehlmann, M. Parente, J. F. Mustard, S. L. Murchie, G. A. Swayze, J.-P. Bibring, and E. A. Silver (2009), Characterization of phyllosilicates observed in the central Mawrth Vallis region, Mars, their potential formational processes, and implications for past climate, *J. Geophys. Res.*, 114, E00D10, doi:10.1029/2008JE003301.

Milliken, R. E. (2007), Clay minerals in water-lain sedimentary deposits in the southern highlands: Evaluating habitability on Mars with MSL, 2nd MSL Landing Site Workshop, NASA, Pasadena, Calif., 23–25 October.

Milliken, R. E., et al. (2008), Opaline silica in young deposits on Mars, *Geology*, 36(11), 847–850, doi:10.1130/G24967A.1.

Morgan, F., F. Seelos, and S. Murchie (2009), CAT Tutorial, presented at CRISM Workshop held in conjunction with the 40th Lunar and Planetary Science Conference, Lunar and Planet. Inst., Woodlands, Tex., 22 March.

Murchie, S., et al. (2007), Compact reconnaissance imaging spectrometer for Mars (CRISM) on Mars Reconnaissance Orbiter (MRO), *J. Geophys. Res.*, 112, E05S03, doi:10.1029/2006JE002682.

Murchie, S. L., et al. (2009a), A synthesis of Martian aqueous mineralogy after 1 Mars year of observations from the Mars Reconnaissance Orbiter, *J. Geophys. Res.*, 114, E00D06, doi:10.1029/2009JE003342.

Murchie, S. L., et al. (2009b), The compact reconnaissance imaging spectrometer for Mars investigation and data set from the Mars Reconnaissance Orbiter's primary science phase, *J. Geophys. Res.*, 114, E00D07, doi:10.1029/2009JE003344.

Mustard, J. F., et al. (2008), Hydrated silicate minerals on Mars observed by the Mars Reconnaissance Orbiter CRISM instrument, *Nature*, 454, 305–309, doi:10.1038/nature07097.

Naumov, M. V. (2005), Principal features of impact-generated hydro-thermal circulation systems: Mineralogical and geochemical evidence, *Geofluids*, 5, 165–184, doi:10.1111/j.1468-8123.2005.00092.x.

Neukum, G., and R. Jaumann (2004), HRSC: The high resolution stereo camera of Mars express. In: Mars Express: The Scientific Payload, *Eur. Space Agency Spec. Publ.*, *ESA SP-1240*, 17–35.

Noe Dobrea, E. Z., et al. (2010), Mineralogy and stratigraphy of phyllosilicate-bearing and dark mantling units in the greater Mawrth Vallis/west Arabia Terra area: Constraints on geological origin, *J. Geophys. Res.*, 115, E00D19, doi:10.1029/2009JE003351.

Osterloo, M. M., V. E. Hamilton, J. L. Bandfield, T. D. Glotch, A. M. Baldridge, P. R. Christensen, L. L. Tornabene, and F. S. Anderson (2008), Chloride-bearing materials in the southern highlands of Mars, *Science*, 319, 1651–1654, doi:10.1126/science.1150690.

Osterloo, M. M., F. S. Anderson, V. E. Hamilton, and B. M. Hynek (2010), Geologic context of proposed chloride-bearing materials on Mars, *J. Geophys. Res.*, 115, E10012, doi:10.1029/2010JE003613.

Paquet, H. (1970), Évolution géochimique des minéraux argileux dans les altérations et les sols des climats méditerranéens et tropicaux à saisons contrastées, *Mém. Serv. Carte Géol. Alsace-Lorraine*, 30, 212 pp.

Parente, M. (2008), A new approach to denoising CRISM images, *Lunar Planet. Sci.*, *XXXIX*, Abstract 2528.

Pelkey, S. M., et al. (2007), CRISM multispectral summary products: Parameterizing mineral diversity on Mars from reflectance, *J. Geophys. Res.*, 112, E08S14, doi:10.1029/2006JE002831.

Pondrelli, M., A. P. Rossi, L. Marinangeli, E. Hauber, K. Gwinner, A. Baliva, and S. Di Lorenzo (2008), Evolution and depositional environments of the Eberswalde fan delta, Mars, *Icarus*, 197, 429–451, doi:10.1016/j.icarus.2008.05.018.

Poulet, F., J.-P. Bibring, J. F. Mustard, A. Gendrin, N. Mangold, Y. Langevin, R. E. Arvidson, B. Gondet, and C. Gomez, and the OMEGA Team (2005), Phyllosilicates on Mars and implications for early Martian climate, *Nature*, 438, 623–627, doi:10.1038/nature04274.

Poulet, F., J.-P. Bibring, B. Gondet, Y. Langevin, J. Mustard, N. Mangold, V. Chevrier, and A. Gendrin (2007), Discovery, mapping and mineralogy of phyllosilicates on Mars by MEx-OMEGA: A reappraisal, Abstract 3170, presented at the Seventh International Conference on Mars, Lunar and Planet. Inst., Pasadena, Calif., 9–13 July.

Quantin, P. (1972), Les andosols: Revue bibliographique des connaissances actuelles, *Cah. ORSTOM Sér. Pédol.*, 10(3), 273–301.

Quantin, P., D. Badaut-Trauth, and F. Weber (1975), Mise en évidence de minéraux secondaires, argiles et hydroxydes, dans les andosols des Nouvelles-Hébrides, après la déferrification par la méthode de Endredy, *Bull. Groupe Fr. Argiles*, 27, 51–67.

Righi, D., and A. Meunier (1995), Origin of clays by rock weathering and soil formation, in *Origin and Mineralogy of Clays*, edited by B. Velde, pp. 43–161, Springer, Berlin.

Roach, L. H., J. F. Mustard, G. Swayze, R. E. Milliken, J. L. Bishop, S. L. Murchie, and K. Lichtenberg (2010), Hydrated mineral stratigraphy of Ius Chasma, Valles Marineris, *Icarus*, 206, 253–268, doi:10.1016/j.icarus.2009.09.003.

Robinson, D., and R. E. Bevins (1989), Diastathermal (extensional) metamorphism at very low grades and possible high grade analogues, *Earth Planet. Sci. Lett.*, 92, 81–88, doi:10.1016/0012-821X(89)90022-8.

Schumm, S. A., J.-F. Dumont, and J. K. Holbrook (2002), *Active Tectonics and Alluvial Rivers*, 292 pp., Cambridge Univ. Press, Cambridge, U. K.

Schwenzer, S. P., and D. A. Kring (2009a), Impact-generated hydrothermal systems capable of forming phyllosilicates on Noachian Mars, *Geology*, 37, 1091–1094, doi:10.1130/G30340A.1.

Schwenzer, S. P., and D. A. Kring (2009b), Impact-generated hydrothermal alteration on Mars: Clay minerals, oxides, zeolites and more, *Lunar Planet. Sci.*, *XL*, Abstract 1421.

Scott, D. H., and K. L. Tanaka (1986), Geologic Map of the western equatorial region of Mars, *U.S. Geol. Surv. Misc. Geol. Invest. Map*, *I-1802-A*, 1:15M scale.

Smith, D. E., et al. (2001), Mars Orbiter Laser Altimeter (MOLA): Experiment summary after the first year of global mapping of Mars, *J. Geophys. Res.*, 106(E10), 23,689–23,722, doi:10.1029/2000JE001364.

Sonnenfeld, P. (1984), *Brines and Evaporates*, 631 pp., Academic, San Diego, Calif.

Swayze, G. A., R. N. Clark, S. J. Sutley, C. A. Gent, B. W. Rockwell, D. L. Blaney, J. L. Post, and B. P. Farm (2002), Mineral mapping Mauna Kea and Mauna Loa shield volcanos on Hawaii using AVIRIS data and the USGS Tetracorder spectral identification system: Lessons applicable to the search for relict Martian hydrothermal systems, in *Proceedings of the 11th JPL Airborne Earth Science Workshop JPL Publ. 03–4*, edited by R. O. Green, pp. 373–387, Jet Propul. Lab., Pasadena, Calif.

Swindale, L. D., and M. L. Jackson (1960), A mineralogical study of soil formation in four rhyolite-derived soils from New Zealand, *N.Z. J. Geol. Geophys.*, 3, 141–183, doi:10.1080/00288306.1960.10423590.

Thollot, P., N. Mangold, S. Le Mouélic, R. E. Milliken, L. H. Roach, and J. F. Mustard (2010), Recent hydrated minerals in Noctis Labyrinthus Chasmata, Mars, *Lunar Planet. Sci.*, *XLI*, Abstract 1873.

Tosca, N. J., S. M. McLennan, D. H. Lindsley, and M. A. A. Schoonen (2004), Acid–sulfate weathering of synthetic Martian basalt: The acid fog model revisited, *J. Geophys. Res.*, 109, E05003, doi:10.1029/2003JE002218.

Velde, B. (1992), *Introduction to Clay Minerals*, 193 pp., Chapman Hall, London, doi:10.1007/978-94-011-2368-6.

Weaver, C. E. (1989), *Clays, Muds, and Shales, Developments in Sedimentology*, vol. 44, 819 pp., Elsevier, Amsterdam.

Weitz, C. M., R. E. Milliken, J. A. Grant, A. S. McEwen, R. M. E. Williams, and J. L. Bishop (2008), Light-toned strata and inverted channels adjacent to Juventae and Ganges chasmata, Mars, *Geophys. Res. Lett.*, 35, L19202, doi:10.1029/2008GL035317.

Weitz, C. M., R. E. Milliken, J. A. Grant, A. S. McEwen, R. M. E. Williams, J. L. Bishop, and B. J. Thomson (2010), Mars Reconnaissance Orbiter observations of light-toned layered deposits and associated fluvial landforms on the plateaus adjacent to Valles Marineris, *Icarus*, 205, 73–102, doi:10.1016/j.icarus.2009.04.017.

Weitz, C. M., J. L. Bishop, P. Thollot, N. Mangold, and L. H. Roach (2011), Diverse mineralogies in two troughs of Noctis Labyrinthus, Mars, *Geology*, 39(10), 899–902, doi:10.1130/G32045.1.

Wintzer, A. E., C. C. Allen, and D. Z. Oehler (2011), Phyllosilicate deposits in Shalbatana Vallis, *Lunar Planet. Sci.*, *XLII*, Abstract 1557.

Witbeck, N. E., K. L. Tanaka, and D. H. Scott (1991), Geologic map of the Valles Marineris region, Mars, *U.S. Geol. Surv. Misc. Geol. Invest. Map*, *I-2010*.

Wray, J. J., B. L. Ehlmann, S. W. Squyres, J. F. Mustard, and R. L. Kirk (2008), Compositional stratigraphy of clay-bearing layered deposits at Mawrth Vallis, Mars, *Geophys. Res. Lett.*, 35, L12202, doi:10.1029/2008GL034385.

Wray, J. J., S. L. Murchie, S. W. Squyres, F. P. Seelos, and L. L. Tornabene (2009), Diverse aqueous environments on ancient Mars revealed in the southern highlands, *Geology*, 37, 1043–1046, doi:10.1130/G30331A.1.

O. Bourgeois, Laboratoire de Planétologie et Géodynamique, UMR 6112, CNRS, Université de Nantes, 2 rue de la houssinière, BP 92208, F-44322 Nantes CEDEX 3, France.

J. Flahaut and C. Quantin, Laboratoire de Géologie de Lyon, UMR 5276, CNRS, Université Claude Bernard Lyon 1, Ecole Normale Supérieure de Lyon, 2 rue Raphaël Dubois, F-69622 Villeurbanne CEDEX, France.

E. Hauber, R. Jaumann, and L. Le Deit, Institute of Planetary Research, DLR, Rutherfordstr. 2, D-12489 Berlin, Germany. (laetitia.ledeit@dlr.de)

D. Mège, J. Gurgurewicz and M. Massé, WROONA Group, Institute of Geological Sciences, Polish Academy of Sciences, Research Centre in Wrocław, Podwale St. No. 75, PL-50449, Poland.